UNIVERSITAT POLITÈCNICA DE CATALUNYA

MASTER THESIS

5G Multi-Antenna Vehicle Scattering Characterization

Author:
Kushal DUMRE

Mentor:
Christian BALLESTEROS SÁNCHEZ

Supervisor:
Prof. Dr. Lluis JOFRE ROCA

A thesis submitted in fulfillment of the requirements for the degree of Masters in Telecommunication Engineering

in the

Signal Theory and Communications Department
Telecom BCN

Escola Tècnica Superior d'Enginyeria de Telecomunicació de Barcelona
UNIVERSITAT POLITÈCNICA DE CATALUNYA
BARCELONATECH

June 20, 2019

UNIVERSITAT POLITÈCNICA DE CATALUNYA

Abstract

Masters in Telecommunication Engineering

5G Multi-Antenna Vehicle Scattering Characterization

by Kushal DUMRE

In today's era of Internet, everything is tending to be intelligent enough to be managed by itself. Following the same line, vehicles are more than vehicular machines. They are tending to be autonomously driven, able to communicate, and gather huge amount of data. For this purpose, vehicles of tomorrow should incorporate technology to be able to handle these requirements. Not only the internal communication, external communication is critical and vital to adapt vehicles in this sophisticated environment of autonomous driving. Connecting the vehicle to the present huge infrastructure is an important and also an interesting challenge.

The main objective of this thesis is to validate a new approach to study the characterization of the scattering of an antenna in the presence of a supporting vehicle. This objective is addressed with the base of Radio Frequency (RF) imaging technique for some potential bands of Fifth Generation Wireless Communication Technology (5G). Studies are performed for different scenarios to validate the proposal.

Acknowledgements

I am using this opportunity to express my gratitude to everyone who supported me throughout the course of the development of this thesis. I am sincerely grateful to them for sharing their truthful and illuminating views on a number of issues related to the project.

First of all, I want to express my sincere gratitude to Prof. Dr. Lluis JOFRE ROCA for his aspiring guidance, invaluably constructive criticism, great opportunities and friendly advice during the project work and during all of the time of this Master program. Without those it would have been very difficult for me to present this thesis.

I would also like to express many thanks to my friend and the mentor of this project, Christian Ballesteros Sánchez, for his countless effort, help and suggestions during the development of this project. I wish him very best luck for his current journey.

I would also like to thank my colleague Badr Bouazza for helping me in uncountable moments during our time in the university.

I would also like to mention all of the professors and staffs from the department and the university for every help and suggestion.

Last but not the least, I thank my family and friends for the immense support. If I have reached my goals, it is just because of you.

Contents

List of Figures

List of Tables

Acronyms

5G Fifth Generation Wireless Communication Technology.

AoI Area of Interest.

CSI Channel State Information.

CST Computer Simulation Technology.

GTD Geometrical Theory of Diffraction.

ITS Intelligent Transportation Systems.

MIMO Multiple Input Multiple Output.

mmW Millimeter Wave.

RF Radio Frequency.

SVD Singular Value Decomposition.

UTD Uniform Theory of Diffraction.

UWB Ultra Wide Band.

V2I Vehicle to Infrastructure.

V2V Vehicle to Vehicle.

VNA Vector Network Analyzer.

Chapter 1

Introduction

This chapter aims to provide the introduction of the project and its main parts developed during the development of this thesis. The principal goal of this work is to study the potential of some of the promising band of 5G by electromagnetic imaging for electrically large objects, into the microwave and millimeter wave (mm-wave) bands. As a consequent step, this thesis provides a feasible approach to study the signature of a radiating antenna on a vehicular platform i.e. the electromagnetic parameters by using the electromagnetic sensors as illustrated in figure 1.1.

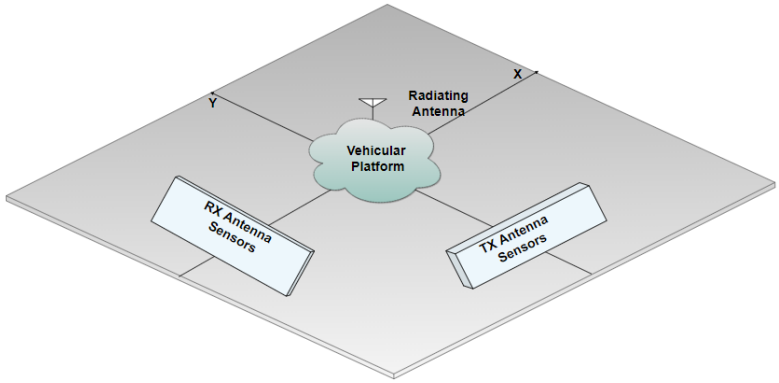

FIGURE 1.1: Multi-antenna vehicle scattering characterization

Based on the imaging techniques using multiple electromagnetic sensors, a method for the characterization of canonical objects and also of a vehicle is proposed.

For the validation of this approach, both numerical and experimental analysis are performed for canonical and realistic platforms. For the canonical analysis, simulation software is used to model and extract the electric fields properties. Measurement campaign is done to validate the RF imaging approach for the reconstruction of the scattering effect.

As a figure of merits, the obtained data is post processed to apply the RF imaging and also to characterize the scatterer to obtain the information of the electric fields. Post processing is explained in detail on how the data obtained from different approach is treated. Presented results validate the proposed method.

1.1 Motivation

Vehicles of today's digital society are smart enough to sense the environment and take actions depending on the circumstances of that, but still not intelligent enough to communicate with each other or even with any another entity by themselves. In terms of autonomous driving, connectivity is required to provide the full freedom to the vehicles, ones from present or the futuristic ones of which we still don't know

how they will look like and what will be their capacity apart from self driving. As they get developed featuring the capacity of communication, probably they will be able to complement one of the current most important technology, cell phones.

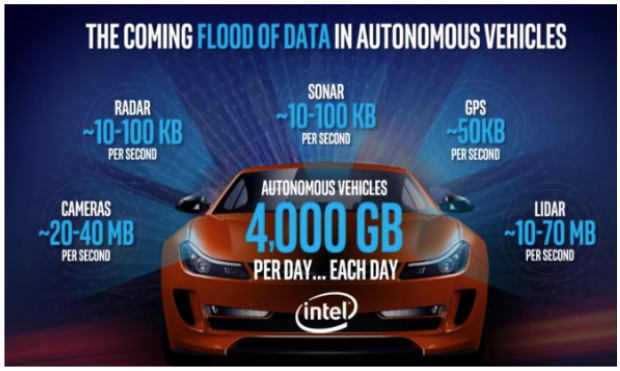

FIGURE 1.2: Estimation of data produced by a futuristic autonomous vehicle [1]

To exploit this "flood of data" as presented in figure 1.2, connectivity of the vehicles is most required . This connectivity should not be limited only for the basic advantages of the autonomous driving but also should be designed to make the vehicles parts of the connected society. For this purpose, it's essential for futuristic vehicles to have gateway to the huge network infrastructure being deployed today and also of the future. Newer concepts and improvements of existing Vehicle to Infrastructure (V2I) and Vehicle to Vehicle (V2V) networks are currently being investigated. But still, vehicles are not able to take advantages of pure V2V communication by being part of the available infrastructure, because only fewer and newer ones, also known as connected vehicles, are equipped with external 4G communication module which is similar to a cell phone. To fulfil the demand of the volume of data to be produced by vehicles, the capacity of communication systems is a important factor that should be taken in account. In the present context to address this solution, multi element antennas are commonly used to increase mainly the bandwidth capacity in the communication links.

Vehicular communication is an important and interesting topic being discussed these days. Big and important actors of the digital society have shown their interest in this emerging sector. For vehicular communications, standards are defined and many investigations are being done for different frequency bands, which are mainly centered in sub 6 and in mmwave band [6]. Taking into account the present standard for Intelligent Transportation Systems (ITS), IEEE 802.11p and also the potential standards being developed in sub-6 GHz band of 5G communication systems, in this thesis both bands are considered as a subject of study. For the vehicular communication, the main motivation to shift to the upper frequency bands is the requirement of lower latency, higher frequency bandwidth and eventually high accuracy target detection [7].

On one hand due to the evolution of 5G and its deployment for numerous application, it will not take longer to have almost everything being connected to each other within the similar criteria in term of regulations, operating compatibility and performance parameters. In other hand, as suggested in [8, 9, 10], the use of the RF signals to sense or characterize the environment are being more attractive day by

day in different field of the industry including mainly in industrial, medical, and security applications. The Main advantage of using the RF signal for source scattering imaging applications is the possibility to have the resolution as small as $\lambda/2$ [11].

1.2 Objectives and Milestones

The main objective of this thesis is to understand the platforms impact in a microwave operator environment. Different frequency bands are considered in this work for the purpose of comparison. To do so, a solid theoretical background, use of different software for calculation and simulation is also required. These objectives can be outlined in following points.

- Investigation of the state of the art: Study the state of the art of scattering characterization.
- Theoretical literature: Understand the theoretical background of the concepts related to this project.
- Software introduction: Understand the basic usage of different softwares to be used during the development of the thesis.
- Pre-experimental approach: This objective is set for numerical analysis of canonical and realistic platform. Modelling and simulation of a simple scenario is done.
- Experimental approach: Measurement campaign setup including hardware requirements such as antennas and measurement devices. Translation of the outcomes from the measurement to the figure of merits presented as results.

1.3 Work Plan

This thesis is divided in main three parts without considering the documentation phase which are as following.

- Investigation : Theoretical literature, state of the art.
- Analysis : Analysis, theoretical and pre-experimental (numerical and simulated).
- Measurements : Measurement campaign, characterization.

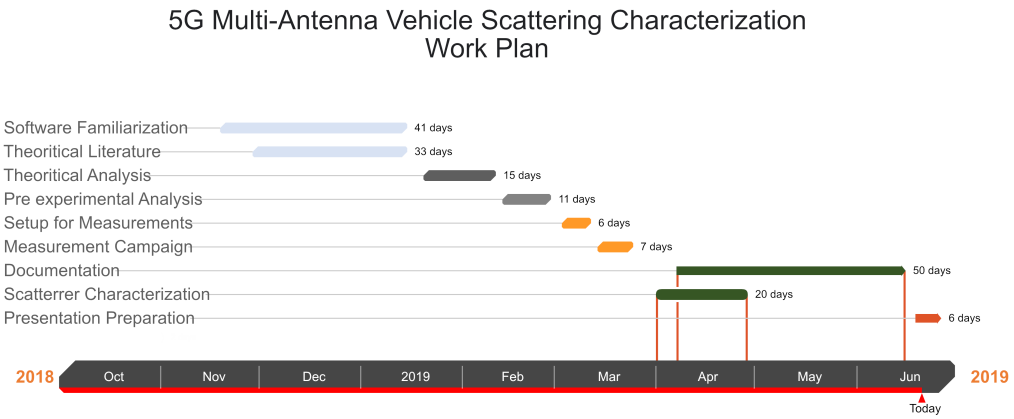

FIGURE 1.3: Gantt chart with main objectives of the master project.

Figure 1.3 illustrates the general work plan of the master thesis with some of the main tasks realized.

1.4 Thesis Organization

This Thesis is organized as in following order.

- Chapter 2 provides the theoretical background referred during the whole development of this project.
- Chapter 3 illustrates the methods used to develop this work, the details of the measurement campaign and the related tasks.
- Chapter 4 describes the pre-experimental approach of this project where canonical and realistic scatterers are studied and also the corresponding results are presented. In this chapter the theoretical knowledge is applied to obtain the basic results.
- Chapter 5 details the procedure and results to characterize the electromagnetic signature of a radiating element positioned over a vehicular platform.
- Chapter 6 presents the conclusion of this thesis based on the results presented in the previous chapters.

Chapter 2

Theoretical background

This chapter provides the general concept of the theoretical literature related to RF imaging using electromagnetic signals. Apart from studying the imaging of scatterers, this work also focuses the study of channels characteristics. In this chapter, basics of Radio frequency transmission and propagation are explained. Then, Ray tracing approach, multiple antenna and more specifically MIMO, and wireless channel characteristics parameters are explained. RF imaging is then explained and followed by this, a concept of vehicle scattering characterization, exploiting the RF imaging, is introduced.

2.1 Basics of Transmission

As a basic and a simpler approach, in terms of complexity, Monopole antenna as transmitting and receiving elements is considered for theoretical study of this work. Monopole antenna are normally situated vertically on z-axis, above the ground plane and with feeding on its base.

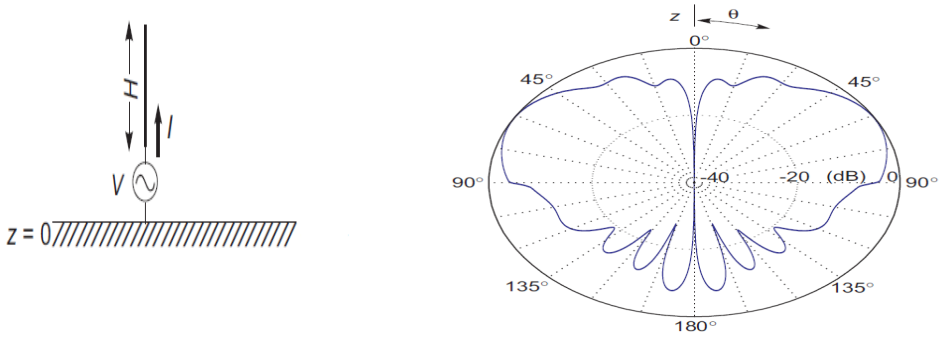

(A) Monopole antenna (B) Radiation pattern of monopole antenna

FIGURE 2.1: Monopole antenna above finite ground [2]

The typical radiation pattern of a monopole antenna over a finite ground plane is illustrated in figure 2.1b, situated as in figure 2.1a, on which the maximum radiation is not at 90°, but instead around 60°- 70°. This change of radiation pattern, compared to the ideal radiation pattern of a monopole antenna over an infinite ground plane (maximum on 90°), is occurred due to the finite ground plane effect. The electric field produced by the monopole antenna is as presented in (2.1) and this equation, for a monopole of $H = \lambda/4$ can be approximated, for the ideal case, as (2.2)

$$E_\theta = j\frac{\eta}{2\pi r}e^{-jkr}I_m\frac{cos(coskHcos\theta) - cosH}{sen\theta}, \qquad E_\phi = 0 \tag{2.1}$$

$$E_\theta = j60\frac{e^{-jkr}}{r}I_m\frac{cos(\frac{\pi}{2}cos\theta)}{sen\theta}, \qquad E_\phi = 0 \tag{2.2}$$

From the above equation, (2.2), resulting phase of the electric field can be extracted. Power received by another antenna placed at a distance r can be calculated from equation of transmissions as in (2.3)

$$P_r = P_t D_t D_r \left(\frac{\lambda}{4\pi r}\right)^2 \tag{2.3}$$

where D_t, D_r is the directivity of transmitting and receiving antenna respectively, which is 3.28 for each [2].

2.1.1 Multipath Propagation

In RF transmission, multipath occurs when a signal takes two or more paths from the transmitting antenna to the receiving antenna. These different paths, reached to the receiving antenna, appears due to reflection, refraction or diffraction caused by an obstacle or a scatterer. When the electromagnetic wave interacts with scatterers, it experiences an amplitude, phase and polarization change, due to which the direct signal usually tends to be more stronger.
For example, if we consider a Gaussian pulse as a transmitted signal in frequency domain, as in the equation 2.4

$$X(f) = Ae^{-2*(\pi*\sigma*f)^2} \tag{2.4}$$

where, A is the amplitude of the signal, σ is the duration of the signal pulse and f is the frequency of transmission.
In the other part, considering the multipath propagation, signal received by the receptor is equivalent to the equation 2.5

$$Y(f) = X(f)e^{j\omega t}\left[\frac{e^{-j\omega t_0}}{r_0} + \frac{e^{-j\omega t_1}}{r_1} + ... + \frac{e^{-j\omega t_n}}{r_n}\right] \tag{2.5}$$

where X(f) is the transmitted signal, ω is the angular frequency in radians, t is time in seconds, t_0 and t_1, and r_0 and r_1 are time of arrival in seconds and distance travelled in meter by a direct ray and a tap respectively. t_n and r_n is the Time of arrival (ToA) and distance travelled by the n^{th} element of multipath respectively. Signal propagation mode and scattering materials characteristics , for example conductivity, affects multipath propagation and path loss [12].

2.2 Ray Tracing

Ray tracing concept in electromagnetic propagation was firstly developed by Pierre de Fermat in 1654, who stated that, "ray takes always the shortest time to travel from one point to another no matter what sort of reflection the ray belongs to "[13]. Electromagnetic rays can be classified into basic types, direct rays, reflected rays and diffracted rays. Furthermore, there exists, other classifications based on combination of these basic rays such as, double diffraction rays, reflected-diffracted rays etc [14].

Based on this basic classification and paths of the ray figure 2.2 shows Fermat's principle for three different paths: AB'C, ABC, and AB''C between the source A and sink C. The wave propagates from A to B and gets reflected towards C because path ABC is the shortest way of travel.

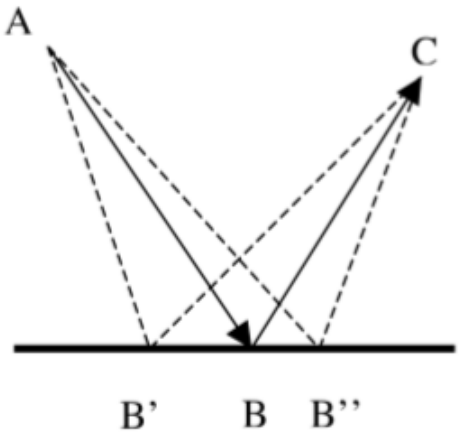

FIGURE 2.2: Fermat principal for basic ray propagation.

Ray tracing approach takes in account the basic classification of electromagnetic rays [15], those mentioned earlier, which are as :

- Direct rays
  Rays with an un-obstructed trajectory between the source and destination.
- Reflected rays
  Rays those which bounce on a smooth mirror surface and thus interacts with different medium.
- Diffracted ray
  A single incident ray generates a large amount of possible diffracted rays when reaching an edge of a rigid body, which are more complex and dynamic compared to the reflected rays.

Figure 2.3 illustrates the reflection and diffraction of the rays while interacting with smooth and rigid surface respectively.

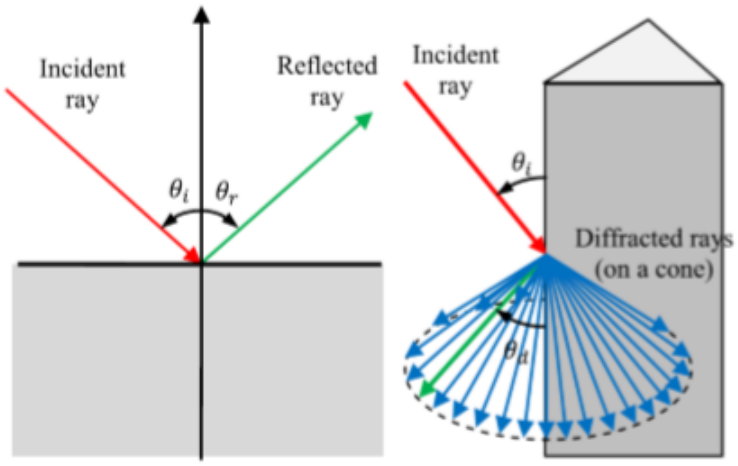

FIGURE 2.3: Rays: Reflected over a smooth surface (left) and Diffracted on interacting with a Edge forming a cone (right) [3]

Taking in account the complexity of the diffraction of electromagnetic rays, different proposals were made to model the diffraction. Some of the famous are, Geometrical Theory of Diffraction (GTD) and Uniform Theory of Diffraction (UTD). The model used by Remcomm Wireless InSite, used in this work, X3D is an enhanced high fidelity ray tracing model which includes reflections, transmissions and diffractions along with frequency dependent atmospheric absorption.

2.3 Communication System With Multiple Antennas

To cope with above mentioned effects in wireless communication, group of antenna is used also known as multiple antennas in transmission, in reception or in both. Multiple antenna technologies have received high attention in the last few decades for their capabilities to improve the overall system performance. The main advantages of using multiple antenna systems are that, they are capable of increasing link reliability and channel capacity and can reduce the interference in both uplink and downlink.

2.3.1 Basic Literature : MIMO

Due to the increasing demand of the high bandwidth and crowded spectrum because of frequency allocation for various application, efficiency of communication channel is explored and exploited. In radio communication systems, Multiple Input Multiple Output (MIMO) is used to improve the channel capacity by using multiple transmission and receiving antennas by taking the advantage of the multipath propagation. Depending on the techniques of this exploitation, from the signal processing approach, MIMO can be divided into 3 sub-categories.

- Precoding
  Also known as Beamforming, is a spatial processing done at transmitter taking in account Channel State Information (CSI), in which the same signal is emitted from each of the transmit antennas with appropriate phase and gain weighting such that the signal power is maximized at the receiver input.This is done through the technique of constructive combination, mainly in terms of

the phase, of the signal emitted from different antennas. The main objective is to increase the received signal gain and to reduce the multipath fading effect.

- Spatial Multiplexing
  Spatial Multiplexing is a powerful technique for increasing channel capacity at higher signal-to-noise ratios (SNR) in which higher rate signal is divided into multiple lower rate streams and each of these streams are transmitted through different transmitting antennas on same channel (frequency).These streams are interpreted by receiving array as parallel streams.Combined with precoding, with the help of CSI, this technique can be used for simultaneous transmission to multiple receivers, also known as Multi user MIMO .

- Diversity Coding
  Diversity coding, without channel information, exploits the independent fading in the multiple antenna links to enhance signal diversity through space-time coding techniques.Space time coding is used to improve the reliability of data transmission using multiple antennas at transmission.

2.3.2 Capacity

A conventional MIMO system can be modelled as in 2.6 where y and x are vectors of recieved and transmitted signal, and H and n are channel response and AWGN noise vector respectively.

$$\mathbf{y} = \mathbf{Hx} + \mathbf{n} \tag{2.6}$$

Depending upon the number of transmitting and receiving elements, above equation can be represented as in 2.7, where each elements of the matrix H represents each propagation path or channel gain for corresponding transmitting and receiving antennas.

$$\begin{bmatrix} y_1 \\ y_2 \\ \vdots \\ y_M \end{bmatrix} = \begin{bmatrix} h_{11} & h_{12} & \cdots & h_{1N} \\ h_{21} & h_{22} & \cdots & h_{2N} \\ \vdots & \vdots & \ddots & \vdots \\ h_{M1} & h_{M2} & \cdots & h_{MN} \end{bmatrix} \begin{bmatrix} x_1 \\ x_2 \\ \vdots \\ x_N \end{bmatrix} + \begin{bmatrix} n_1 \\ n_2 \\ \vdots \\ n_N \end{bmatrix} \tag{2.7}$$

In information theory, channel capacity is referred as the maximum transmission rate with very minimal error probability[16]. For a generic MIMO system with ideal coding, the maximum channel capacity can be represented as in equation 2.8 below.

$$C = log_2\left(det\left[I_N + \frac{P_T H H^*}{P_N}\right]\right) \tag{2.8}$$

where, H is $M_r \times N_t$ channel matrix normalized to the Forbenius norm, P_T and P_N are transmitted power and noise power at reception respectively. This expression also can be expressed as in 2.9, in terms of eigenvalues i-th element of a matrix resulting from the product between H and its transpose conjugate[17].

$$C = \sum_{i=1}^{N} log_2\left(1 + \frac{P_T \lambda_i}{P_N}\right) \tag{2.9}$$

Depending on the statistical properties of the channel, the ergodic capacity is no greater than the number, N = min(N_t, N_r) times larger than that of a SISO system.

On a MIMO system, for a analysis purpose one of the common approach is to study the correlation of the channel matrix by its channel condition number. The condition number can be calculated with the largest and lowest eigenvalue as in the following equation [18].

$$||H||F = \sqrt{\sum_{m=1}^{M}\sum_{n=1}^{N}|H_{MN}|^2} \tag{2.10}$$

$$CN(db) = 20log_{10}\frac{\lambda_{max}(||H||F)}{\lambda_{min}(||H||F)} \tag{2.11}$$

where λ_{max} and λ_{min} correspond to the maximum and the minimum non zero eigenvalue of the normalized channel matrix, respectively. $||H||F$ indicates the Forbenius normalization of channel matrix H as illustrated in equation 2.10. A small channel condition number indicates low correlation and consequently higher channel capacity.

2.3.3 Correlation

Theoretically, the capacity of MIMO systems improves by increasing the number of transmitting and receiving antenna elements when the channel gains are uncorrelated [19] as a consequence of their channels' decomposition into an equivalent set of parallel spatial sub-channels. On the other side, signal correlation limits the achievable capacity of MIMO system resulting negative effect of exploitation of diversity technique [20]. The main factor to have signal correlation, in realistic environment, is due to insufficient antenna spacing and sparse scattering environments which decreases the spread angle. So, to avoid the signal correlation, while grouping of the antennas for a better angle spread smaller inter-element distance is needed as can be seen in figure 2.4. But in other hand, the trade off of this situation is mutual coupling between the antennas, which has negative impact in channel capacity.

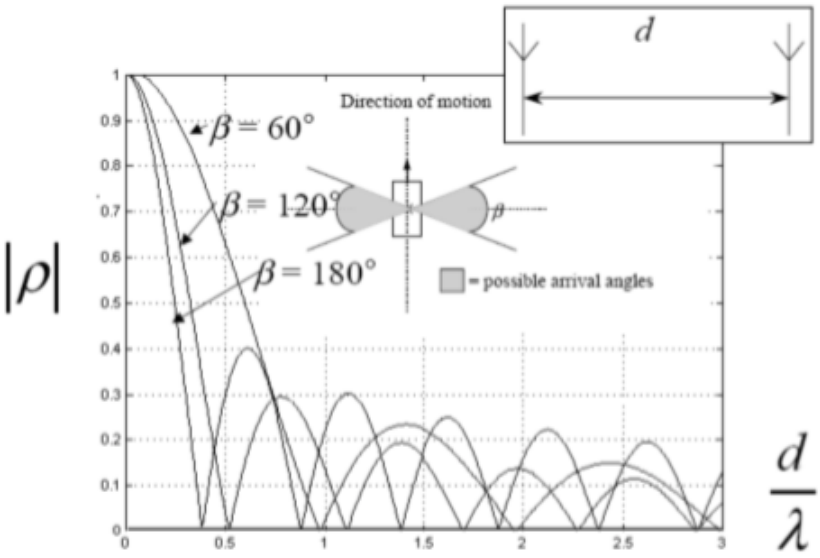

FIGURE 2.4: Correlation for two dipoles with changing inter-element spacing and three distinct angle of arrival.[4]

2.4 Characteristics Parameters of Wireless Channel

Eigenvalues are one of the common terms in analysis of linear transformations. As mentioned in the name, the prefix *eigen* comes from the German language which means proper or characteristic. Originally it was used by physicist-mathematician Euler in 18th century to study principal axes of rotation of rigid body [21]. Currently eigenvalues and eigenvectors have wide range of application such as vibration analysis, atomic orbitals, facial recognition, matrix diagonlization, signal processing and electromagnetic characterization. In signal processing and electromagnetic characterization, some of the major applications are

- Number of significant communication channel in MIMO.
- Spatial location of the dielectric objects or scatterers.

2.4.1 Eigenvalues and Eigenvectors

In linear algebra, an eigenvector or autovector, of a linear transformation, is known as non-zero vector which is changed only on scalar factor when that linear tranformation is applied on it.

Theorem

If T is a linear transformation from a vector space V over a field F into itself and v is a vector in V that is not the zero vector, then v is an eigenvector of T if T(v) is a scalar multiple of v. This condition can be written as the equation

$$T(\mathrm{v}) = \lambda \mathrm{v} \tag{2.12}$$

where λ is a scalar in the field F, known as the eigenvalue, characteristic value, or characteristic root associated with the eigenvector v.

2.4.2 Singular Value Decomposition

Singular Value Decomposition (SVD) is a linear algebraic approach used for a factorization of a real or complex matrix.In other terms, it is also defined as eigendecomposition of symmetric matrix with positive eigenvalues to any $m \times n$ matrix. Eigendecomposition, is known as factorization of diagonalizable matrices into a canonical form where it is represented only in terms of eigenvalues and eigenvectors.

Theorem

For a $m \times n$ matrix M,with elements, from the filed K, of either real or complex numbers, there exists a algebraic factorization as following.

$$M = U\Sigma V^* \tag{2.13}$$

- U is a $m \times m$ unitary matrix over K , unitary matrices are orthogonal matrices),
- Σ is a diagonal $m \times n$ matrix with non-negative real numbers on the diagonal,
- V is an $n \times n$ unitary matrix over K, and V^* is the conjugate transpose of V.

The diagonal entries δ_i of matrix Σ are known as Singular values of M. These singular values, are non negative real numbers and commonly listed in descending order. For a given matrix M, if non null eigenvalues of $M^H M$ are λ_i, then $\sqrt{\lambda_i}$ are the singular values of M [22].

2.5 Scatterer Characterization

Imaging or mapping technique consists in representing the scattered electromagnetic field between number of electromagnetic sensors (mainly transmitters and/or receivers) on a certain region, covering as much as possible the area on which RF mapping is to be done [9, 23]. The main objective is to obtain the spatial and electrical information of the extended object ε_r relative to the original background constant ε_b of the Area of Interest (AoI) S_o, with an object or a scatterer as shown in figure 2.5.

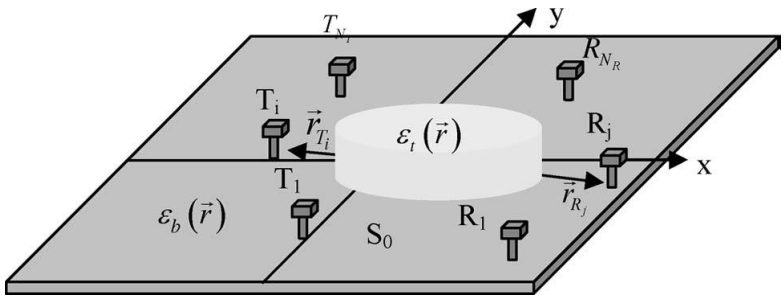

FIGURE 2.5: Scatterer mapping technique sensing geometry

The equivalent electric current distribution induced on AoI when the scatterer is illuminated with an electromagnetic field generated by the transmitter located at the distance of $\vec{r}_{T_i}$ at a frequency f, i.e., $E(\vec{r}, f; \vec{r}_{T_i})$, is proportional to the electrical contrast $c(\vec{r}) = (\epsilon_t(\vec{r}) - \epsilon_b)/\epsilon_b$ and it is defined as:

$$J_{eq}(\vec{r}, f; \vec{r}_{T_i}) = j\omega\epsilon_b c(\vec{r}) E(\vec{r}, f; \vec{r}_{T_i}) \tag{2.14}$$

On an AoI with a set of M_T transmitting elements and M_R receiving element, the scattered field received by a receiver positioned at $\vec{r}_{R_j}$ created by the equivalent current $J_{eq}(\vec{r}, f; \vec{r}_{T_i})$ can be expressed as:

$$E_s(\vec{r}_{R_j}, f, \vec{r}_{T_i}) = -j\omega\mu_0 \int_{Vo} J_{eq}(\vec{r}, f; \vec{r}_{T_i}) G(|\vec{r}_{R_j} - \vec{r}|, f) dV \tag{2.15}$$

where $G(|\vec{r}_{R_j} - \vec{r}|, f)$ is the Green's function for the particular 2D or 3D geometry. The main difference is that, some vertical formulation based on 3-D Green function should be used to compensate the effects like vertical diffraction and depolarisation, caused due to the object inhomogeneities in the z-axis.

For the reconstruction or imaging of the scatterer, the AoI is reconstructed to form image points by means of focused group of antennas, of transmitters and receivers. As a reconstruction algorithm, the resulting scattered field matrix E_s is mathematically treated with corresponding weights over each specific point of the reconstruction area. This focusing algorithm restores the changes in phase and amplitude of waves travelling from transmitting antenna to the analyzed point and then to the receiving antenna. These electromagnetic waves suffer the corresponding amplitude and phase propagation changes modulated by the refraction and diffraction due to the presence of the scatterer. Applying the compensating focusing algorithm on the

channel matrix for all points of the space grid, a replica of the environment to be reconstructed is obtained.

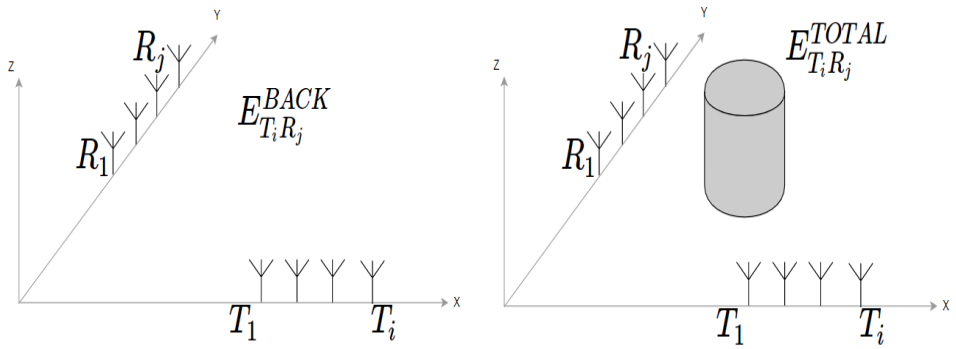

(A) Electric field without scatterer (B) Electric field with scatterer

FIGURE 2.6: Reconstruction a scatterer

Also, the scattered field E_s can be expressed as in equation 2.16, where $E^{TOTAL}_{T_iR_j}$ is the total electric field with the presence of the scatterer and $E^{BACK}_{T_iR_j}$ is the electric field only of the scenario in a free space conditions, as seen in figure 2.6.

$$E_s = E^{TOTAL}_{T_iR_j} - E^{BACK}_{T_iR_j} \tag{2.16}$$

In terms of sampling in frequency domain systems, minimum number of views N_ϕ should be respected to guarantee no loss of the information. N_ϕ is equal to the number of coefficients of cylindrical mode expansion of the scattered field.[9] This results in a maximum angular step $\Delta\phi$ as shown in equation 2.17. Also to mitigate with the aliasing problem appropriate frequency step must be chosen as in equation 2.18.

$$\Delta\phi = \lambda_{min}/(2a) \tag{2.17}$$

$$\Delta f = \frac{c_0}{4(a+\delta_a)} \tag{2.18}$$

where, λ_{min} is the minimum wavelength, c_0 is the propagation velocity of the light, a is the radius of a circle encircling the object and δ_a is a margin of delays to be considered.

Furthermore, using the channel properties obtained during the reconstruction, characterization of the wireless channel over AoI can be done by obtaining parameters such as the eigenvalues and eigenvectors of the scattered fields matrix [24]. Following the same approach as by authors in the paper[25], using the SVD method characteristics parameters (eigenvalues and eigenvectors) of the whole scenario under investigation can be obtained. These parameters relate to the main scatterers spatial position indicating the source of the scattered electric field E_s.

$$E_{SM_T \times M_R} = U_{M_T \times M_T} \Sigma_{M_T \times N_R} V^T_{N_R \times N_R} \tag{2.19}$$

where the columns of U are the left eigenvectors related to the transmission array, S is a diagonal matrix including the eigenvalues and V^T is the transpose matrix of the right eigenvectors, related to the receiving array. Total number of these eigenvectors corresponds to the number of antennas in the arrays of transmission and reception corresponding to T and R respectively.

2.6 Signature Characterizations of an Antenna on Vehicular Platform

Exploiting the RF imaging concept used in scatterer characterization, as a next step in this work, the signature of the radiating element over the vehicular platform is studied. The main objective is to extract the information of the distribution of equivalent electric current induced by the radiation antenna.

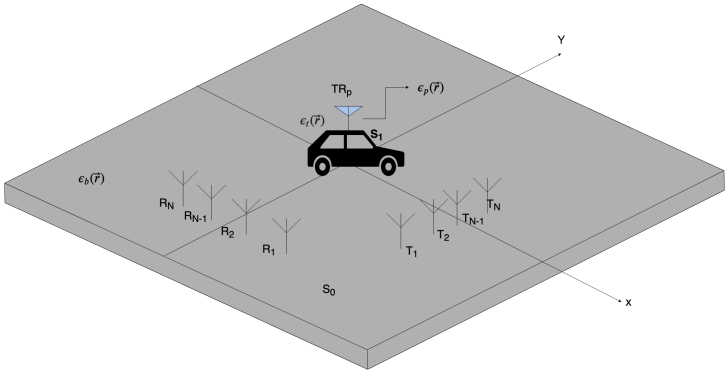

FIGURE 2.7: Enhanced Scatterer characterization technique sensing geometry

In this case, our objective is to obtain the electrical information of the extended object ε_p relative to the original background constant ε_t over the scatterer surface S_1 as shown in figure 2.7.

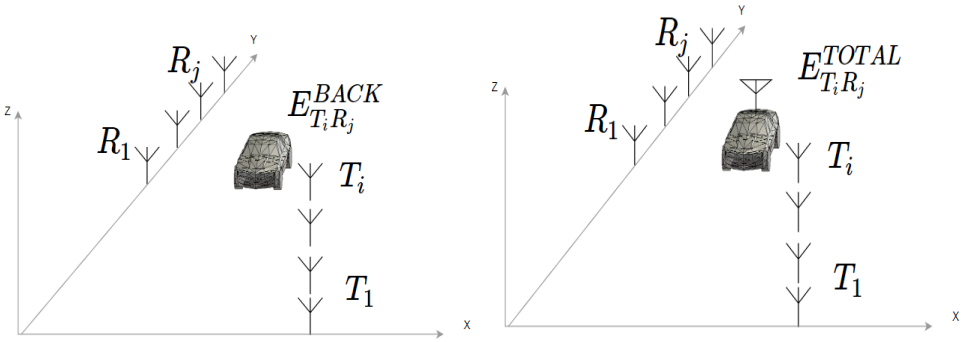

(A) Electric field without scatterer (B) Electric field with scatterer

FIGURE 2.8: Radiating element footprint over the vehicular platform using multi-sensor arrays for imaging

In this case, the electric field produced by the passive radiating element E_{ant}, which can be calculated as in equation 2.20.

$$E_{ant} = E^{TOTAL}_{T_iR_j} - E^{BACK}_{T_iR_j} \tag{2.20}$$

where, $E^{TOTAL}_{T_iR_j}$ is the total electric field produced with the presence of the radiating element over the vehicular platform and $E^{BACK}_{T_iR_j}$ is the electric field produced only in the presence of the vehicular platform, for example a vehicle as represented in figure 2.8.

Using the same algorithm as before for the characterization of the scatterer, contributed values of the phase and the amplitude of the electromagnetic waves due the radiating antenna are restored. This distribution of electric current can be considered equivalent as of active radiating element, in other words a transmitting antenna over the vehicular platform.

From this approach, characteristics of the radiating element over the scatterer can be done through the imaging process. The main advantage of using this technique is that, no any sophisticated measurement system is required to study the complex electromagnetic properties over the surface of any platform such as, equivalent electric current distribution proportional to the electric field produced by the antenna.

Chapter 3

Methodology

The following chapter presents the methodology used in this work. The preface gives a general overview of the main steps and tools used in order to obtain the results. This is followed by the description of two different approach of this work, theoretical and experimental. Measurement campaign is described in detail from basic setup to the operation. Finally, data processing is explained, which provides the general idea of how the radiation parameters obtained from both approaches are dealt to apply the imaging algorithm and for the result presentation.

3.1 Preface

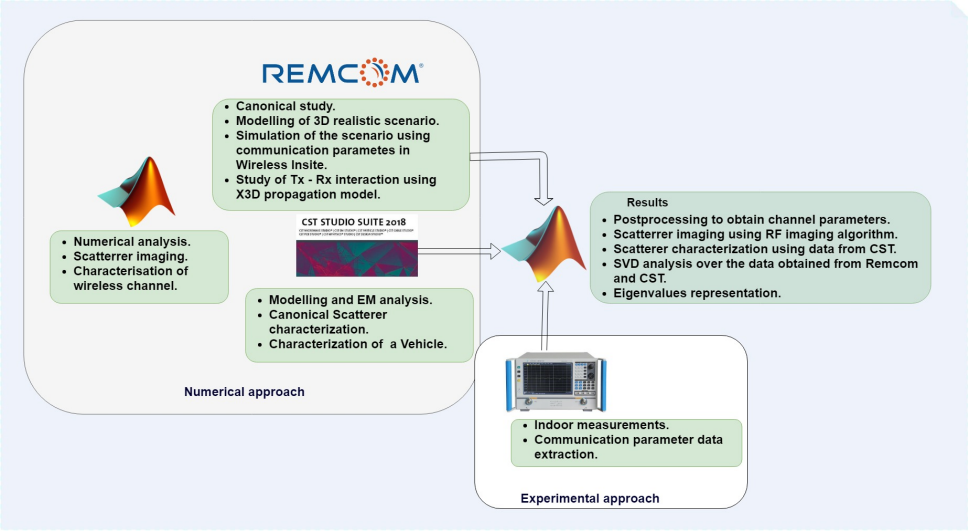

FIGURE 3.1: General representation of main steps of workflow followed the programs used for this work and the programs used.

Figure 3.1 represents the main steps of the workflow followed to develop this thesis. First, for a theoretical approach, *MATLAB* is used for numerical analysis of focusing and scattering mapping techniques as explained in chapter 4.2. Later, as a pre-experimental approach, simulation is done in two phases, at first for RF imaging *WirelessInsiteRemcom* [1] is used, which uses X3D propagation model, to model and study the characteristics of a wireless channel in a modelled scenario and later, *CST studiosite*18 [2] is used to characterize the scatterer in presence of radiating element or antenna. At last and as a final task, for a measurement campaign, a scenario with a scatterrer, is set up where the Vector Network Analyzer (VNA) is used to measure the channel response affected by the scatterer and other parameters of the scenario between multi element transmitting and receiving antenna.

[1] Remcom is a wireless propagation software developed by Wireless Insite
[2] CST is a 3D electromagnetic simulation software developed by Dassault systems

Data obtained from all of the above mentioned approach were post processed in *MATLAB*. This post-processing basically consists on scatterer imaging algorithm application and in some case, calculation of characteristics parameters of the channel through the Singular Value Decomposition (SVD) analysis.

3.2 Numerical Approach

As a major part of the development of this work, after the literature of the state of the art and necessary theoretical background, different canonical structures are analyzed, as well asa realistic vehicular platform. For a numerical analysis, concepts and the formulae presented in chapter 2 are developed in *MATLAB* over which RF imaging and mapping techniques are applied. After the theoretical approach, for a more reasonable study, a simple scenario was modelled in *Remcom*, to obtain the communication and electromagnetic parameters, which are to be used later in post processing to obtain the figures of merit presented as results. For a more detailed study of the electromagnetic effects, mainly the current distribution, of the scatterer in presence of a radiation element, CST is used. The main reason to choose, *CST StudioSite* instead of *Remcom*, is to take advantage of the computational time and the usage experience.

3.3 Experimental Approach

As an experimental approach of this work, different simulations and measurement campaign are performed. A measurement campaign is done to validate the pre - experimental study from which theoretical and simulation results were obtained.

Depending on the development of the work, different figures of merits and different scenarios are considered more relevant and thus presented in this work basically in aspect of the information that could be extracted.

3.4 Measurement Campaign

As a part of the experimental approach, over the completion of theoretical and simulation study, below described measurement campaign is carried out during the development of this thesis. This campaign is performed in same order as below.

3.4.1 Antenna Setup

Conical Ultra Wide Band antenna designed by the authors [5, 26]are used as transmitting and receiving antennas which are able to cover a wide frequency range from 2 to 35 GHz with similar characteristics for whole range. These individual antennas forms the part of electromagnetic sensors to be set up.

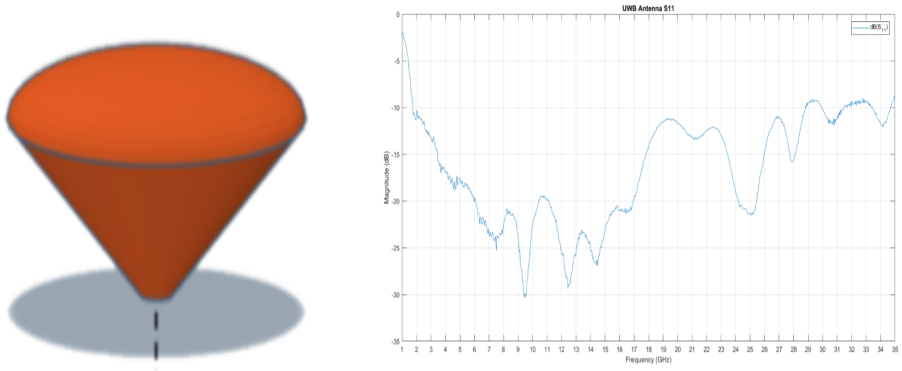

(A) UWB Antenna (B) S_{11} parameter

FIGURE 3.2: UWB antenna, physical structure and frequency response [5].

As seen in the figure, for frequency range of 3 - 4 GHz ($f_{central} = 3.6GHz$) and 24 - 30 GHz ($f_{central} = 26GHz$), promising frequency range of emerging 5G communication, S_{11} parameters are below -15 dB.For curious readers, its highly recommended to check more details about this antenna and whole designing and manufacturing process [5].

3.4.2 Scenario Setup

For the measurement process, multiple conical antennas are mounted up over a metallic ground plane with same separation for transmission and reception, which are placed in an orthogonal coordinates of the scenario where the measurement is performed. For the measurement of channel, i.e. $S-parameters$, N5247A PNA-X VNA is used, in which transmitting and receiving antennas are connected on respective ports as shown in figure 3.3. Measurement scenario is set up inside an anechoic chamber [3] and VNA is operated from outside.As a target firstly, a metallic cylinder was used.

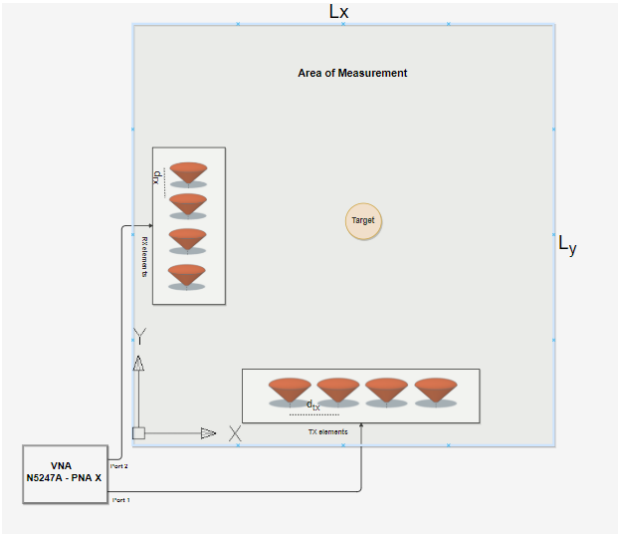

FIGURE 3.3: Overview of measurement scenario with antennas and a single scatterer in the centre

[3]It is not necessary to perform the measurement inside an anechoic chamber as the electric field not related to the scatterer can be compensated during post-processing.Furthermore, doing so all of the scatterer characteristics can be studied. In this work, it is done inside an anechoic chamber as scattering characterization of a specific element is studied.

As shown in the figure above, on two ports of the VNA transmitting and receiving antennas placed on X and Y axis [4] respectively are connected through the coaxial cable which is previously evaluated for the correct functionality in the operating frequency. Before the feeding point of the antenna, the cable passes through the switch from which transmitting/receiving element from the arrays of the antennas can be selected depending upon the specific case of measurement. This switch is implemented for both arrays of antennas and is also evaluated previously for the frequency ranges and is used for the selection of a specific antenna for Tx - Rx purpose on each array. The dark gray color represent the area of measurement which is also the anechoic chamber.

3.4.3 Measurement Data Obtainment

VNA is set-up to operate from the outside of the area of measurement, from where measurement data is stored, which will be post processed in $MATLAB$ to obtain the figures of the merit. For each case of measurement, two different measurements is taken; one with scattering element/s and another without any scattering element in the scenario. As in the post processing only the contribution of scattering element is taken, these measurements data are used to eliminate the the free space electric field and only use the scattered field.

These results are processed to determine the scattering source of the electric fields i.e. scatterer itself through the eigenvectors representation and imaging algorithm.

3.5 Data Post Processing

Once the information about electromagnetic behaviour in presence of the scatterer is extracted through the simulation and measurement, post processing is done, in $MATLAB$, to apply the RF imaging algorithm so to characterize the scatterer.

[4] The coordinates of the location of the antenna are referred as X and Y axis respectively for tx and rx antennas during the whole work and are relative to the scenario

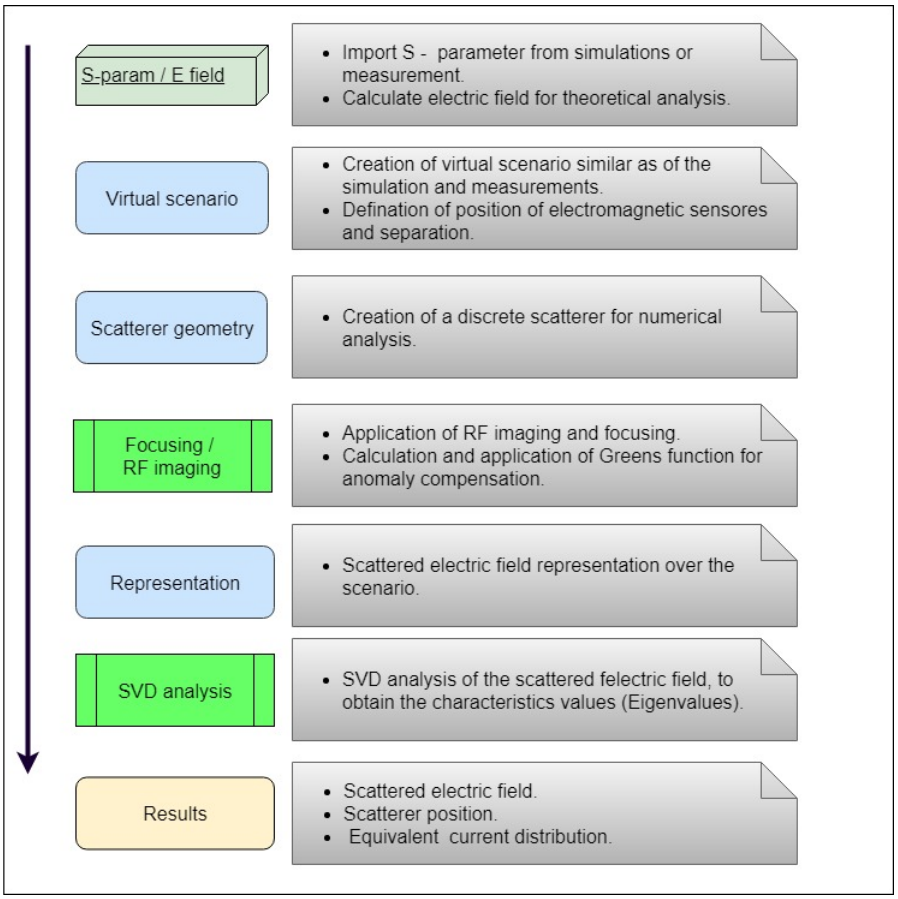

FIGURE 3.4: General information of data processing

The post processing is illustrated in figure 3.4[5] where propagated electric fields or scattering parameters (s-parameters) between transmitting and receiving antennas is used as input. This information source, either is obtained through the simulation or from the measurement campaign. For the theoretical studies, it is calculated numerically. After this, the virtual scenario is defined to construct the electromagnetic arrays (transmitting and receiving antennas), their position and the separation between the antennas. This virtual scenario is constructed in accordance with the geometry of the scenario used in the simulation and defined during the measurement campaign. After that, for the characterization purpose, scatterer geometry is imported as 3D file to be used as mesh over which the distribution of equivalent electric currents is to be projected.

After the definition and creation of the geometry, Focusing is applied to the input in order to construct the scattered electric field which is used for RF imaging. As next step the result of RF imaging is represented, constructing the replica of the scatterer through which the scattered field is generated. Over this electric field, SVD analysis is done, to obtain the characteristics parameters which represent the reflectivity caused by the scatterer in the scenario. As result, position of the scatterer is obtained which is also the source of the scattered electric field and also the equivalent electric field distribution over the scatterer when a radiating element is placed.

[5]Light colored rectangles represents the methods done, bright green color represents the algorithm and analysis performed and the input parameter is represented by a cube.

Chapter 4

Scatterer Imaging

As a pre-experimental approach on this work, based on the theoretical background mentioned on chapter 2, characterization of a scatterer is done using RF imaging technique is done. As a first milestone, analysis of a discrete scatterer is done and later analysis of the canonical geometrical structures, which consists of study of general and simple geometrical objects such as a smooth cylinder, so thus to validate the results. For this, following scenario as of in the figure 4.1 is taken as reference.

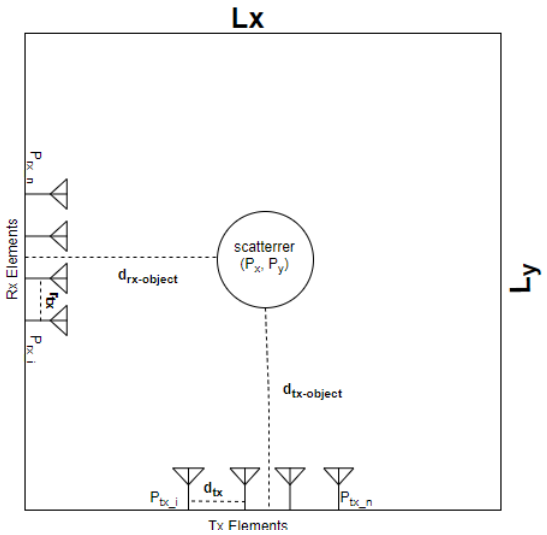

FIGURE 4.1: Scenario of Area of Interest (AoI), where the distance $d_{tx-object}$ and $d_{rx-object}$ is different for each antennas depending on their position.

Arrays of sensors antennas are placed orthogonally over the scenario with a scatterer in it. Distance between antennas of each array corresponds to the half wavelength for different cases, sub 6 or mmwave band. The scenario consists of the dimensions of 50 cm $\times$ 50 cm and the center of the arrays of the sensors antennas are on the center of each axis forming the boundary of the scenario.

4.1 Preface

For this approach, first numerical analysis is done completely in $MATLAB$ and later analysis of a canonical objects is done by the help of the simulation software. For the validation of the outcome of the results obtained, experimental approach is performed. Later to obtain the figure of merits, post processing is done.

4.2 Numerical Analysis of Discrete Scatterer

In this section, a theoretical scenario of dimension $50cm \times 50cm$ with scatterer as an object and 4×4 transmitting and receiving elements is created. Discrete delta is used as the scatterer for the numerical analysis. In the scenario as of figure 4.1, electric field received by the receiving element is as following

$$\vec{E_\theta} = \frac{e^{(-jkd_{tx-obj})}}{d_{tx-object}} \frac{e^{(-jkd_{rx-obj})}}{d_{rx-object}} \tag{4.1}$$

where $k = \frac{2\pi}{\lambda}$ is the wavenumber and the distance between object to transmitting and receiving element are

$$d_{tx_i-obj} = \sqrt{(P_y)^2 + (P_x - P_{tx-i})^2}, \qquad d_{rx_i-obj} = \sqrt{(P_x)^2 + (P_y - P_{rx-i})^2} \tag{4.2}$$

this distance of equation 4.2 is calculated for each transmitting and receiving antenna, depending on number of antennas i.e. from i to n. $P_{tx-i})$ and $P_{rx-i})$ are the axis distance of the specific transmitting and receiving antenna of the respective arrays. If measured from the center of the array, this relative distance is different for each antenna because of the separation between antennas.

Once obtained the electric field, imaging algorithm is applied for the reconstruction of the object as explained in 2.15, using inverse Greens' function for phase compensation. The phase compensation consists on, applying the correction factor of the phase produced due to the propagation due to the distances d_{tx_i-obj} and d_{rx_i-obj}. Inside the Area of Interest (AoI), scattering object is placed in different position to validate the result for different scenario. As explained earlier, using the channel characteristics parameters object position is determined using eigenvectors.

4.2.1 Sub 6 GHz band

For a sub-6 GHz band of 5G, frequency range from 3 - 4 GHz was chosen for the analysis in this work. Inter-element distance between the antennas is set to $\frac{\lambda}{2}$, 5 cm considering the frequency 3 GHz.Transmitting and receiving antennas are placed at the centre of the respective coordinates, horizontal and vertical respectively.In total three study cases were done by changing the position of the scatterer.Studied scenario and the results obtained for each case are presented below.As figure of merit, eigenvector representation and result of imaging algorithm are presented below for each scenarios.

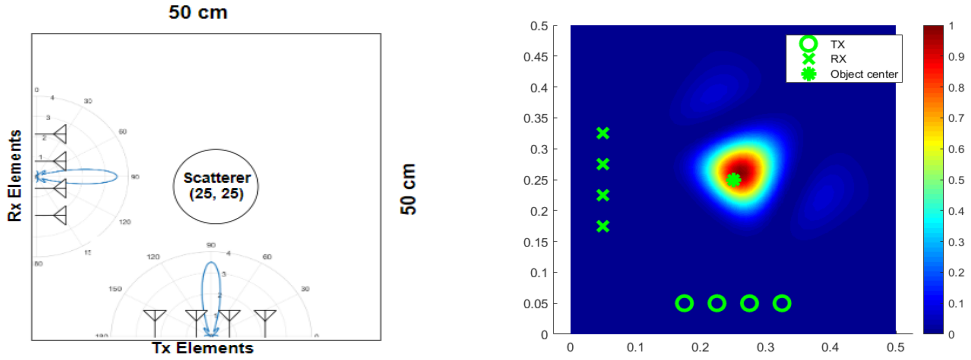

(A) Eigenvectors (B) Reconstructed object

FIGURE 4.2: Object located at the centre of AoI $P_x, P_y = 25cm, 25cm$

As represented above, in figure 4.2a, when the scatterer is placed in the centre of the scenario, resulting eigenvector of the transmitting and receiving antenna points towards the centre i.e. location of the scatterer. And in figure 4.2b the result of the imaging algorithm is

represented, which in some extent, as per the intensity of the colors, gives the location of the scatterer.

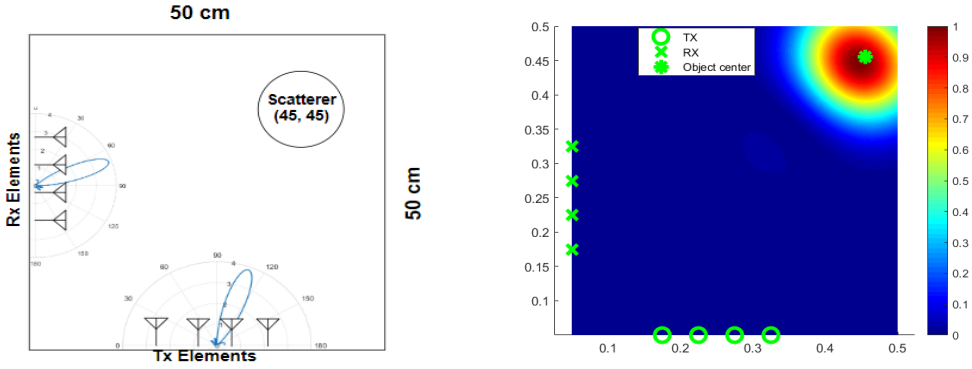

(A) Eigenvectors (B) Reconstructed object

FIGURE 4.3: Object located at top right of AoI $P_x, P_y = 45cm, 45cm$

In this case, location of the scatterer is changed from the centre to the top right corner, further from both transmitting and receiving antenna. Due to which, resulting eigenvectors pointing is also moved as the scatterer as in figure 4.3a. Similarly, as in previous case, the result of imaging algorithm, in figure 4.3b depict the position of the scatterer.

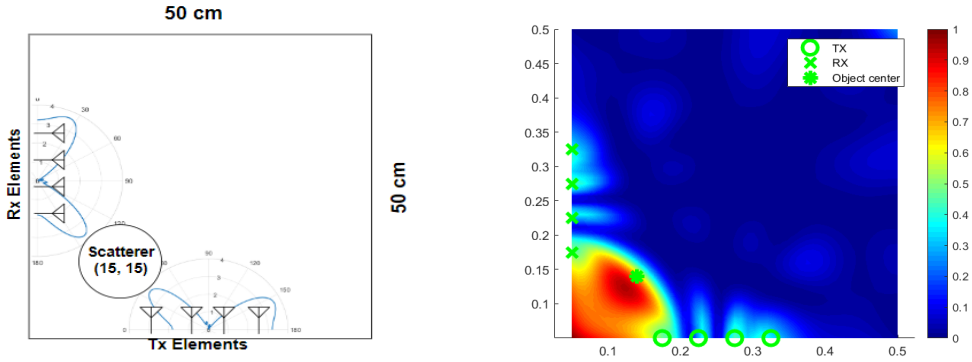

(A) Eigenvectors (B) Reconstructed object

FIGURE 4.4: Object located at bottom left of AoI $P_x, P_y = 15cm, 15cm$

To study another case, scatterer in the left bottom of the scenario i.e. closer from the transmitters and receivers. Eigenvectors representation as in figure 4.4a points towards the scatterer but in presence of one secondary lobe. However the result of imaging algorithm, validates the position of the scatterer.

In all of the results obtained above, Eigenvectors for each scenario point towards the scatterer from where the scattered electric field E_s is obtained. Reconstructed image of the scatterer represents the its exact position. In the plots of scatterer imaging, linear scale is used to color the result, where the highest value is 1 and the lowest in 0. In terms of colors, this values corresponds to dark red and dark blue respectively. In other terms, these values also can be associated as the presence of the scatterer i.e. highest value, dark red, to the centre of the scatterer and the lowest value, dark red, to the empty space.

In third case, figure 4.4, the reconstructed image is not as precise as in other cases which is due to the position of the scatterer between first transmitting and receiving antennas and in very closer distance. It can be observed that, first elements of the arrays of the sensor antennas have higher impact as total distance of propagation is comparatively lower, which contributes to the magnitude and the phase of the generated scattered electric field.

4.2.2 Millimeter Wave band

For this study, frequency range from 24 GHz to 30 GHz was chosen with steps of 600 MHz to make the frequency sample ($N_f = 11$) same as in sub - 6 GHz band.The separation between the antennas is reduced to 5 mm for the geometrical symmetry and more importantly respecting the criteria of separation of $\frac{\lambda}{2}$ corresponding to the frequency 30 GHz.In figures below, for each scenario, eigenvector representation and results obtained after focusing algorithm are presented.

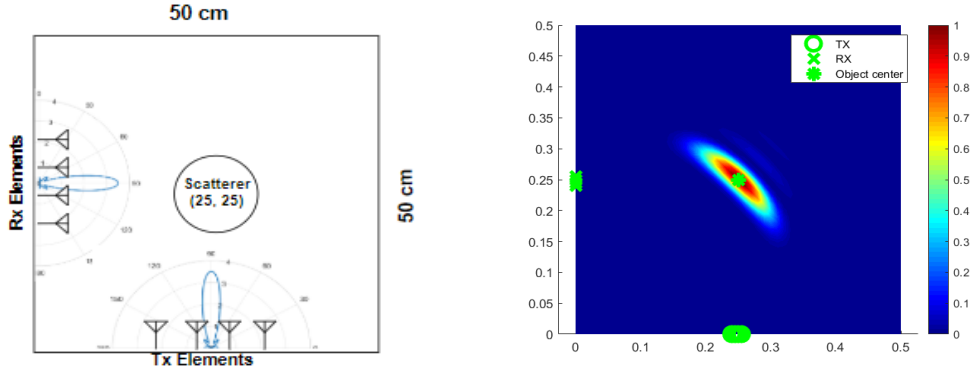

(A) Eigenvectors (B) Reconstructed object

FIGURE 4.5: Object located at the centre of AoI $P_x, P_y = 25cm, 25cm$

For the scatterer located at the centre of the scenario, resulting eigenvectors and the result of imaging algorithm depict the location of the scatterer.Similar as in the same case of the previous part, both results of the figure 4.5 gives the information about the presence of the scatterer located at the centre of the scenario.

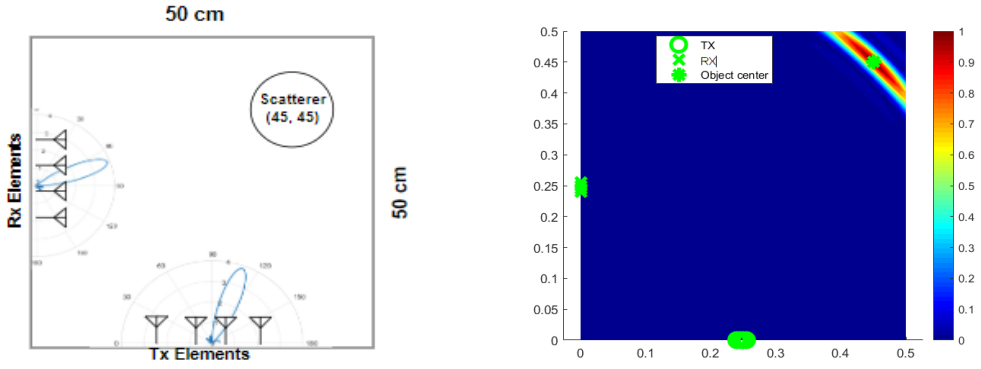

(A) Eigenvectors (B) Reconstructed object

FIGURE 4.6: Object located at top right of AoI $P_x, P_y = 45cm, 45cm$

In this case, the scatterer is moved to the top right corner. After calculating the electric field affected due to the scatterer imaging algorithm is applied. The results of eigenvectors representation and imaging of figure 4.6 reflects the source of scatterred electric field and the position of the scatterer respectively.

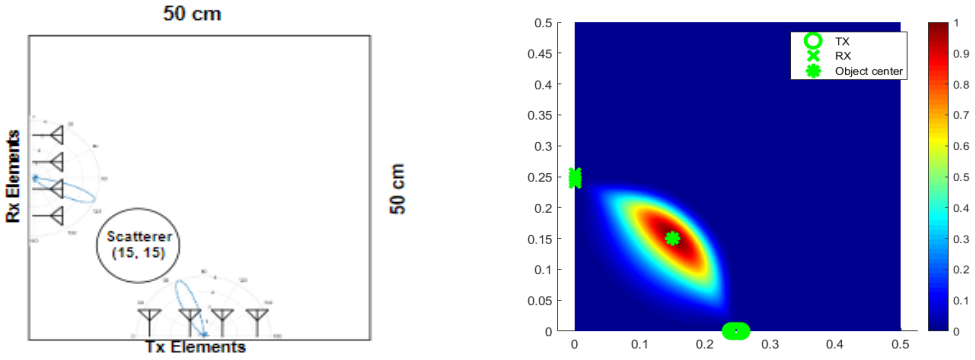

(A) Eigenvectors (B) Reconstructed object

FIGURE 4.7: Object located at bottom left of AoI $P_x, P_y = 15cm, 15cm$

As the last case for the theoretical study, the scatterer is moved to the left bottom of the area making it closer to the antennas.Results of the figure, 4.7 illustrates the eigenvectors and imaging of the given scatterer. Difference to the results obtained for the sub - 6 GHz for same scenario as in figure 4.4, in this case the secondary lobe doesn't appears on eigenvectors representation.

In this result for sub-30 GHz band, both focusing algorithm and eigenvectors have better results in terms of resolution of the reconstructed object. One of the main reason for this improvement is due to the increase of the frequency, which can be translated to the smaller wavelength and this leads to the improvement of the longitudinal resolution. Due to this, reconstructed images are more realistic, the illuminated region is around the object and the resulting images is more cleaner as compared to the results of sub-6 GHz band. For the same reason, as the transverse resolution remains same the resulting images of the scatterer can be observed a bit stretched as compared to the results of the lower frequency band, where the images were more circular. Another thing to be noted is that, as the inter-element distance of the sensor arrays is smaller in this frequency band (almost 10 times smaller), resulting illumination of the same unchanged scatterer is of degraded shape.

4.3 Analysis of Canonical Scatterers

As a second approach of pre-experimental analysis, theoretical scenario defined previously, as in figure 4.1 was modelled in Wireless Insite Remcomm to obtain the electric fields in the presence of the scatterer. As a transmitting and receiving elements, MIMO with monopoles antennas are placed orthogonally in a same plane (XY) to each other as represented in figure 4.8. As a scatterer, octagonal cylinder is used. In this approach, two different scenarios, with a single and two scatterers, for both sub-6 and mmW bands is modelled. In Remcomm, this model is simulated to obtain the electric field which is later processed in MATLAB to use for the focusing algorithm and also to calculate the channels characteristics parameters, eigenvalues and eigenvectors.

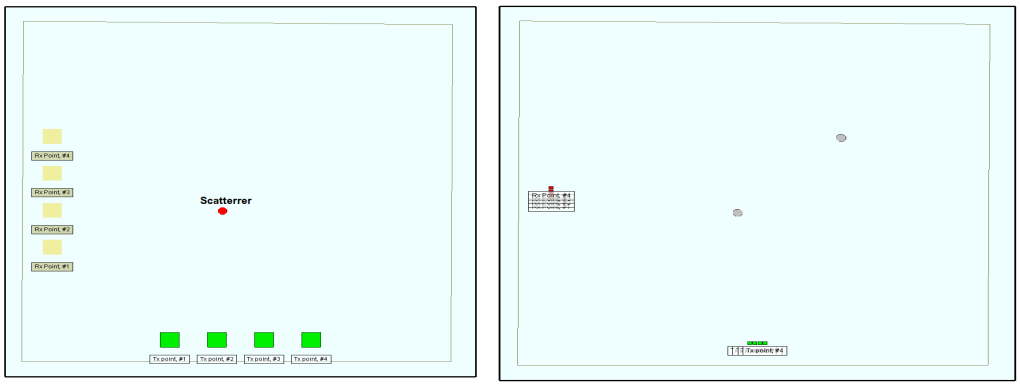

(A) Modelled scenario for sub-6 GHz with 1 scatterer (B) Modelled scenario for Millimeter Wave band with 2 scatterers

FIGURE 4.8: Modelled scenarios in Remcomm

Transmitting and receiving antennas are modelled as points and are placed orthogonally on a same plane with a corresponding distance of separation depending on the frequency range. Some of the parameters of modelling and simulation are illustrated in table below. Properties of propagation model i.e. X3D, used by Remcomm, is set to maximum as shown in table 4.2.

Parameter	**Value**
Distance between Tx/Rx elements (d_{tx}, d_{rx})	$\frac{\lambda}{2}$
Transmission Power (P_{tx})	0 dBm
Frequency range (f)	3 - 4, 24 - 30 GHz
Frequency samples ($\Delta f_{high}, \Delta f_{low}$)	11 (100 , 600 MHz)

TABLE 4.1: Overview of main simulation parameters

Propagation model	X3D
Number of transmission paths	1
Number of reflection paths	2
Number of diffraction paths	13

TABLE 4.2: Overview of propagation model parameters used in *Remcomm*

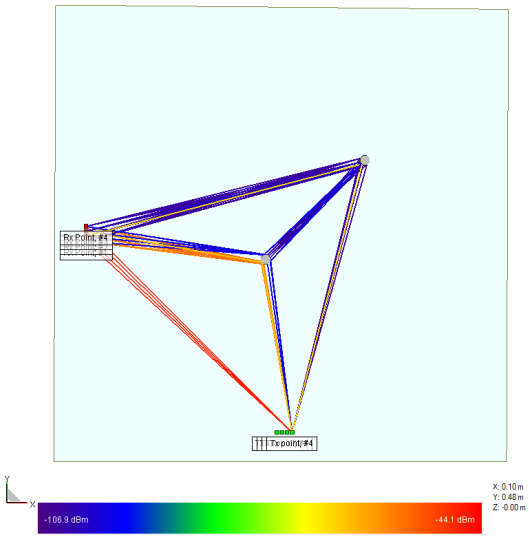

FIGURE 4.9: Propagation paths of the rays with 2 scatterers in the scenario, for the mmwave frequency range

Figure 4.9 illustrates one of the output of the simulation software *Remcomm*, propagation paths, which indicates the number of rays from one transmission point $(TX_{point} = 4)$ and reached to all of the receivers. As a scatterer, two identical metallic cylinders of 1 cm diameters are places in two different positions of the diagonal of the scenario. In red color, direct rays between transmitter and receivers can be observed while in orange and blue are the rays reached to receivers after interacting with a single and both scatterers respectively. These interactions leads to the decrease of the power when they reach to the receivers, this power change can be observed in the color of each rays following the legend of the figure. The strongest ray (direct ray) arrives with $-46.73\ dBm$ while the weakest ray (after interacting with two scatterers in following order, transmission - diffraction - diffraction - diffraction - reception) arrives with $-106.50\ dBm$.

4.3.1 Sub 6 band

In this section, results of the scatterer imaging for sub 6 band are presented.

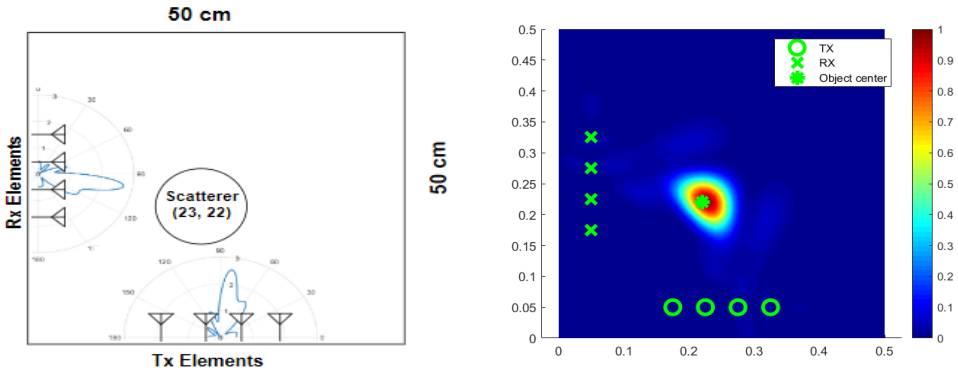

(A) Eigenvectors (B) Reconstructed object

FIGURE 4.10: Reconstruction of 1 scatterer

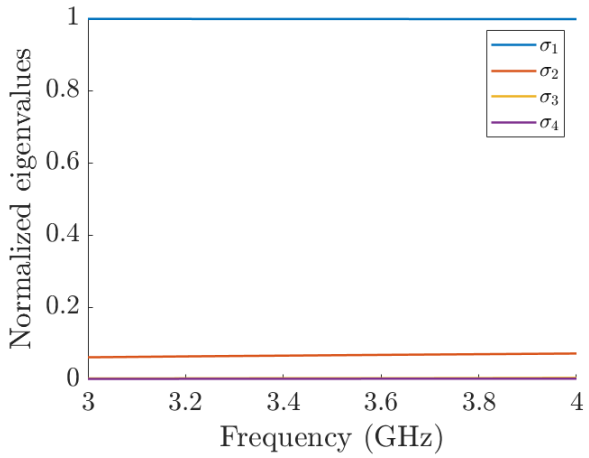

FIGURE 4.11: Eigenvalues representation for sub 6 frequency range with 1 scatterer in the scenario

Above results represent the results for the simulated scenario where a single scatterer is placed in the centre. Figure 4.10 illustrates the eigenvectors representation and the imaging of the scatterer respectively. Figure 4.11 depict the eigenvalue, which characterize the channel, for the whole frequency band used for the simulation. Number of significant eigenvalue, as seen in figure 4.11 conforms the presence of the single scatterer in the scenario. Curiously also a non significant eigenvalue can be observed which is remarkably lower to be unconsidered as compared to the significant one..

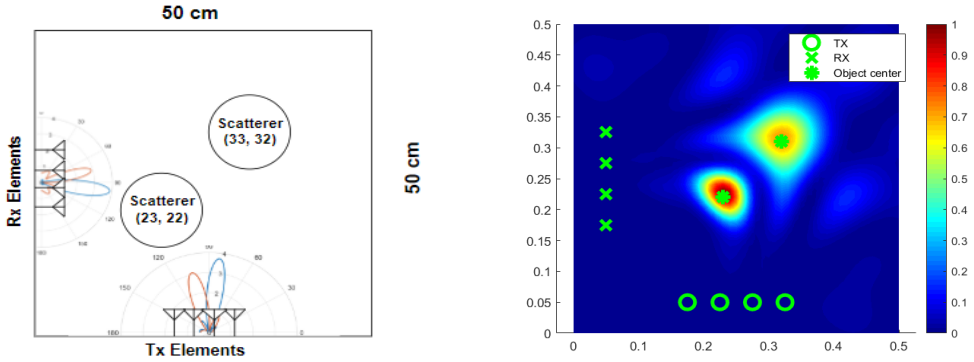

(A) Eigenvectors (B) Reconstructed object

FIGURE 4.12: Reconstruction of 2 scatterers

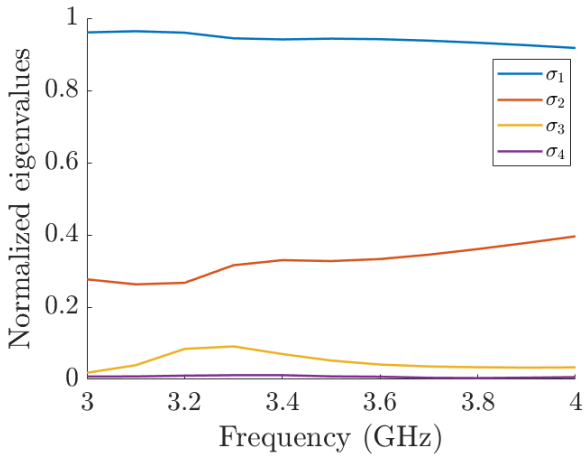

FIGURE 4.13: Eigenvalues representation for sub 6 frequency range with 2 scatterers in the scenario

In this case, instead of only one scatterer in the centre, the scenario is modeled with two scatterer. Similar as in the previous case, figures above represents the scatterer position through eigenvectors representation and imaging plot. The eigenvalues as of the figure 4.13 also represents the presence of the scatterer but in terms of reflectivity. Two significant eigenvalues represents the presence of two reflectors or in other words source of the scattered electric field in the scenario. Resulting number of interactions is higher in terms of propagation due to the presence of two scatterers.

4.3.2 Millimeter Wave band

In this section, results of the scatterer imaging for mmW band are presented.

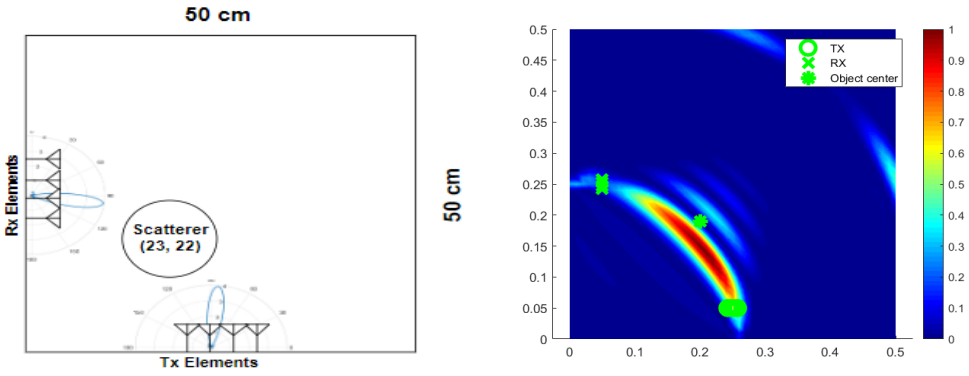

(A) Eigenvectors (B) Reconstructed object

FIGURE 4.14: Reconstruction of 1 scatterer

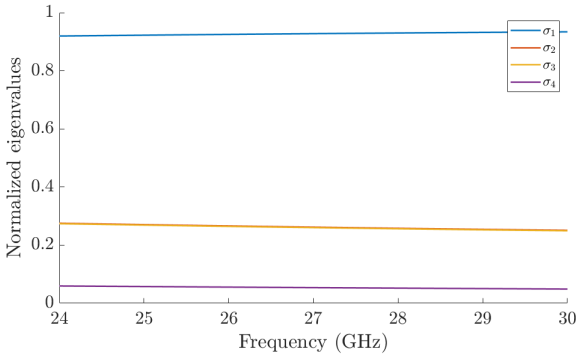

FIGURE 4.15: Eigenvalues representation for frequency range of 24 - 30 GHz with 1 scatterer in the scenario

Similar as in the results for sub 6 band, the scatterer position is indicated by the figure 4.14. A notable change that can be observed is the improvement of the longitudinal resolution, which leads toward certain deformation of the illuminated region. This illuminated region indicates the location of the scatterer. Also to be mentioned that, non significant eigenvalues have higher value as compared to the similar case of sub 6 results which is contributed by higher value of the frequency, or the smaller wave length of the signals.

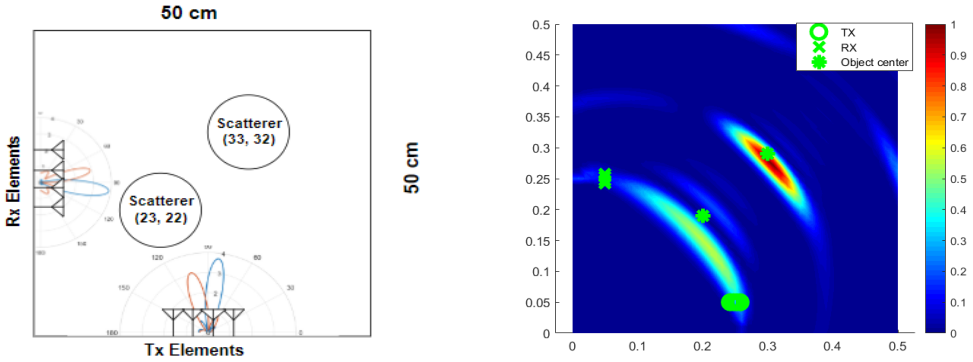

(A) Eigenvectors (B) Reconstructed object

FIGURE 4.16: Reconstruction of 2 scatterers

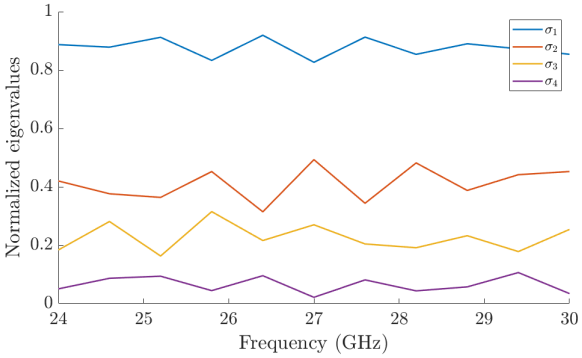

FIGURE 4.17: Eigenvalues representation for sub 6 frequency range with 2 scatterers in the scenario

Results obtained from above simulation depict the location of two scatterer. Each eigenvectors of figure 4.16a points towards the position of the scatterer, which were located during

the simulation. Eigenvalues, as of the figure 4.17 represents the major interactions of the electromagnetic rays travelling from the array of transmitters to the receivers passing through the both of the scatterers.

As can be observed, figures illustrating eigenvalues, for example in 4.15 and 4.17 represents the evolution of eigenvalues along the frequency range. Also it may be observed that, each scatterer contributes with an eigenvalue whose level depends on the relative illumination among them. Total number of significant non-null eigenvalues is an indicator of the reflectivity of the environment, which is directly proportional to the presence of the scatterer in that environment [27].

4.4 Experimental Validation

In this point, after the pre - experimental study, to validate the proposed approach of construction of the scatterer, experimental approach is done. All of the studies realized before in the previous chapters are performed in a real environment using the available resources.

This chapter relates in detail the measurement campaign performed, as explained previously in Measurement Campaign 3.4. At first, scenario setup is explained and after that, results for different studies are presented in respective parts.

4.4.1 Scenario Setup for Measurement

As an experimental approach of this work, measurement campaign was carried out in a similar scenario as of the theoretical approach. Both sub-6 and sub-30 GHz band was covered in single measurement thanks to the Ultra Wide Band (UWB) antennas. This chapter points up the main tasks realized during this campaign and final results obtained.

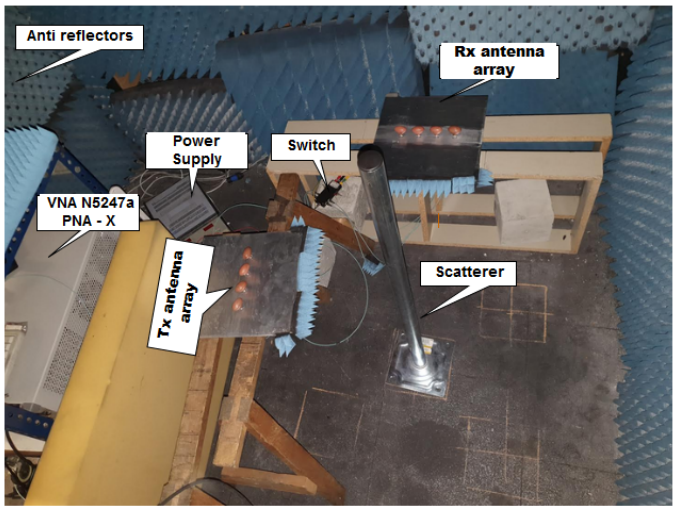

FIGURE 4.18: Measurement scenario setup

Figure 4.18 illustrates the scenario setup details done during the measurement campaign. Above case is for the measurement of electric fields with a single scatterer positioned in the centre of the scenario inside the anechoic chamber. Results form the measurement campaign are presented below in this section. VNA is set up to operate from the outside, even though switching of the antennas of both transmitting and receiving, is done manually. Also, for the measurement of two different electric field, of the free space and with the presence of scatterer, scatterer is taken off manually for every combination of transmitting and receiving antenna.

Parameters	Value
Frequency range	3 - 4 GHz
Number of points (frequency sample)	11 (100 MHz)

TABLE 4.3: Frequency parameters for the measurements

During the measurement campaign, complex value of the electric field is taken for all the frequency span up to 40 GHz. But only the better results, for lower frequencies i.e. sub-6 band are presented. During the data post processing, only the desired values as mentioned in the table 4.3 are considered.

4.4.2 Single Scatterer

As a first approach of experimental approach, 1 scatterer was placed in different location of the scenario so thus to apply focusing algorithm for image reconstruction. In following figures, results for different cases are presented.

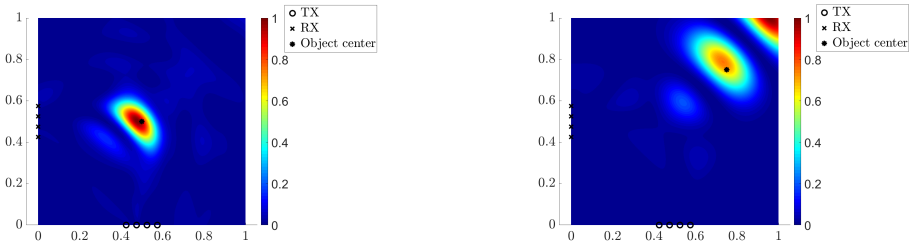

(A) Imaging of the scatterer placed at the centre $P_x, P_y = 25cm, 25cm$

(B) Imaging of the scatterer placed at the upper part $P_x, P_y = 75cm, 75cm$

FIGURE 4.19: Imaging of a single scatterer located on two different positions of the scenario

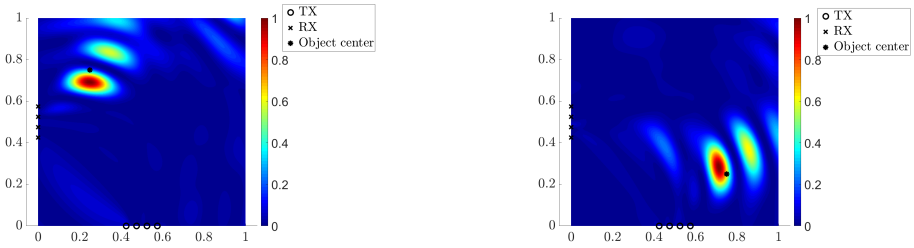

(A) Imaging of the scatterer placed at the upper - left corner $P_x, P_y = 25cm, 75cm$

(B) Imaging of the scatterer placed at the bottom - right corner $P_x, P_y = 75cm, 25cm$

FIGURE 4.20: Imaging of a single scatterer located on a symmetric distance from the receiving 4.20a and transmitting 4.20b antennas.

In above figures, results for the different cases depending upon the position of the scatterers are presented. In figure 4.19, scatterer is placed in two different position among the diagonal of the scenario and in figure 4.20 scatterer is placed near the axis of transmission and reception antennas.

As seen in the results, on every case position of the scatterer is as indicated in the figures. But in case of the second results, as in figure 4.20, presence of the replica of the scatterer can be observed.

4.4.3 Two Scatterers

After the measurement and reconstruction of 1 scatterer in different positions of the scenario, for further validation of the RF imaging, 2 scatterers are used. Results obtained are presented in the figure 4.21.

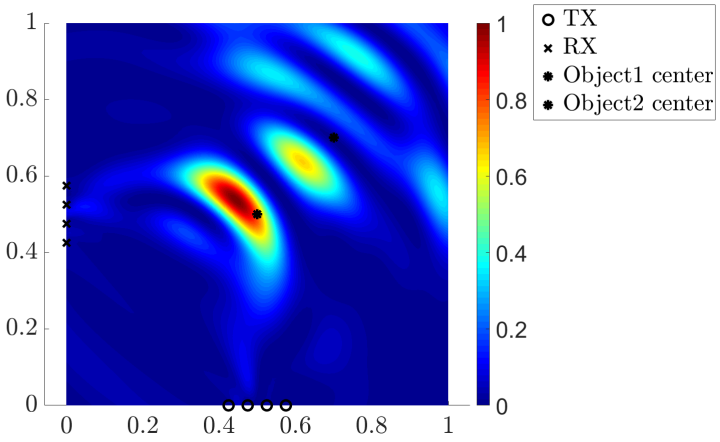

FIGURE 4.21: Imaging of 2 scatterers

Figure 4.21 illustrates the potential positions of the scatterers located in the scenario. Two illuminations can be observed which indicates the possible but not very precise positions of the scatterer. Some other residual illuminations can be obesrved in all results, but mainly in 4.20 in the case, where a single scatterer in placed near to the sensor antenna array.

On both results form the experiment and the simulations, such type of anomaly are present when using multiple scatterers. This type of preliminary results, motivates towards the correction of those by improving the measurement system or through the correction mechanism during the data post processing. In this work, further improvement of this anomaly is not treated.

Chapter 5

Scatterer Characterization

Taking advantage of the the concept of scatterer imaging, as a next step, characterization of the antenna current signature on vehicles is obtained. This characterization of the current signature of an antenna placed on the vehicle using differential scattering technique consists on study of the electric current produced by the passive radiating element, when it is illuminated by electromagnetic waves. In this work different geometrical structure as vehicular platforms, both canonical and real, are considered from a metallic sphere to a scaled car with a realistic geometry. The modelled vehicle and all geometries are fully metallic. In a real life situation, a vehicle is not fully metallic. So this factor should be considered while comparing to the realistic car.

5.1 Preface

In this chapter, the electromagnetic characterization of an antenna on a scatter is presented. To obtain this characterization, at first only the electromagnetic scattering behaviour produced by the vehicular platform is studied and later the electromagnetic behaviour of the scatterer along with the radiating element was studied. For this study, CST studio site 2018 was used for modelling and to obtain the radiation parameters. At first, the characterization study is done using canonical structures as vehicular platforms, for example a sphere and a cylinder. And then, a 1:25 scaled vehicle is used.

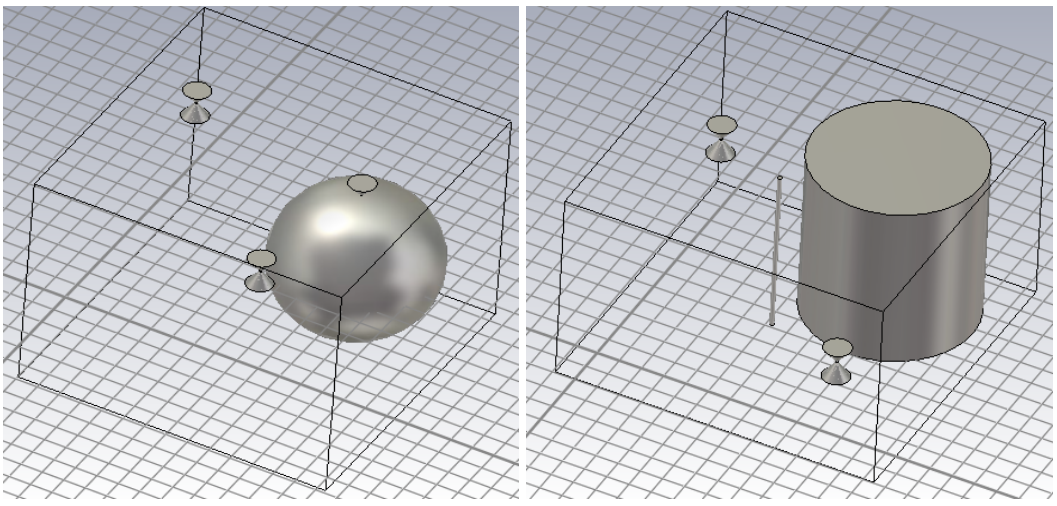

(A) Simulated sphere in CST with a passive monopole on the top (north pole).

(B) Simulated cylinder in CST with a passive dipole in the lateral part.

FIGURE 5.1: Geometry of canonical structure used for characterization

In above figures, two different canonical objects, (a metallic sphere 5.1a and a metallic cylinder 5.1b designed in CST) with radiating element are shown which were modelled in

the simulation software. On the edges of the box of the figures, on each axis transmitting and receiving antenna can be seen which were used as electromagnetic source and sensor.

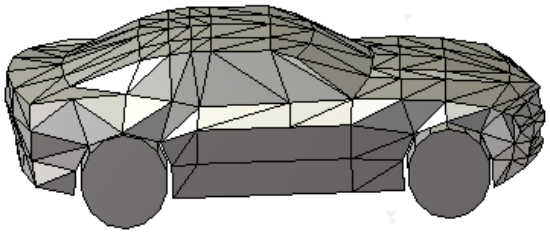

FIGURE 5.2: Simulated car in CST

A scaled car, as in figure 5.2 is used for the simulation to study the characterization in two different cases. In the first case, a short-circuited monopole is placed in the roof of the car and in the second case, a short-circuited dipole is placed on the side of the car, the position of the side mirror of the car.

Array of transmitting and receiving antennas are placed orthogonally as electromagnetic sensores to acquire the electromagnetic information of the scenario. This sensing consists on intercepting this information which is only contributed by the obstacles in the scenario by eliminating other contributions like direct communication link between these antennas, static reflecting obstacles.

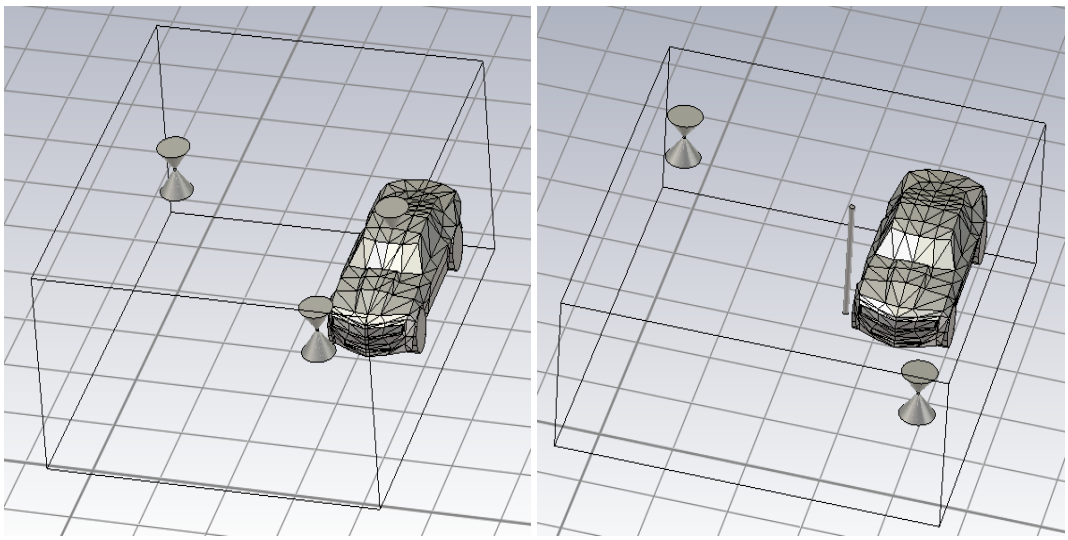

(A) Simulated car in CST with a passive monopole on the roof

(B) Simulated car in CST with a passive dipole in the lateral part.

FIGURE 5.3: Simulation scenario of a vehicle in CST

Depending upon the position of the radiating elements, transmitting and receiving antennas are placed differently to study the resolution in the relevant plane. When a short-circuited antenna, a monopole with ground plane as a scatterer itself, is placed on the top of the vehicular platform, sensing antennas are placed orthogonally on different plane. Transmitters in XZ plane and receivers in XY plane to extract the information of electric current on the roof. When a short-circuited antenna, a dipole , is placed on the lateral part of the vehicular platform, sensing antennas are placed orthognally on same plane i.e. both transmitters and receivers on XY plane to study the distribution of electric field and current in the lateral side.

5.2 Characterization of Canonical Structures

In this section, results of the characterization of the canonical structures are presented. The results presented provides the current distribution information for two different bands, sub-6 and mmwave bands, where the frequency values are of 2-4 GHz and 26-30 GHz. respectively.

5.2.1 Sub 6 GHz Band

For the sub 6 GHz band, results from the simulations done in CST are present below. Parameters, such as separation between transmitting and receiving antennas, passive antennas dimensions are adapted to 3 GHz band.

Data	2 GHz	3 GHz	4 GHz
Amplitude	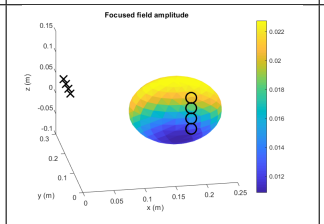	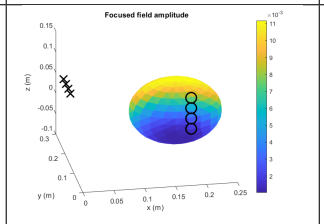	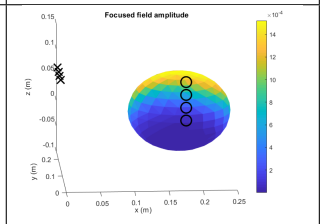
Phase	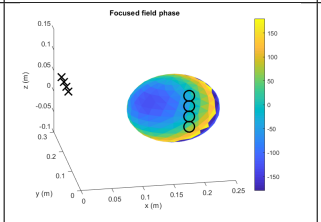	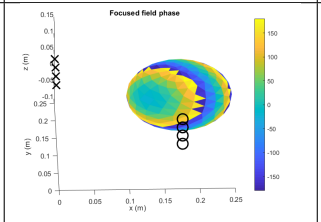	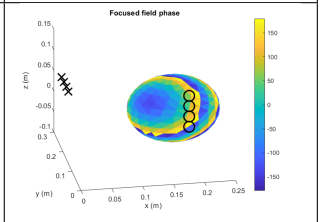
Amplitude	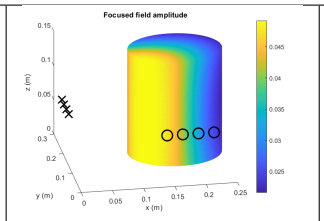	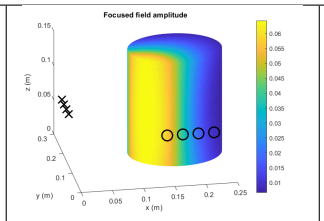	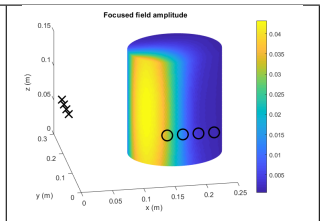
Phase	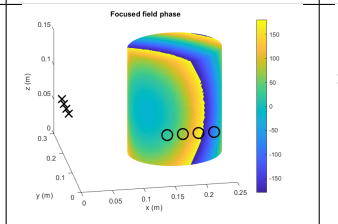	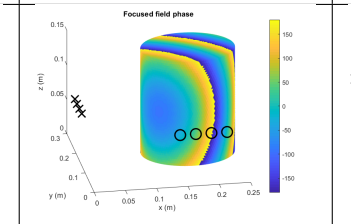	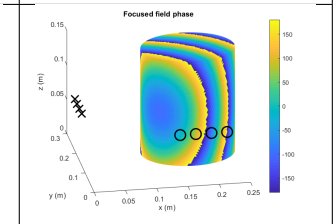

TABLE 5.1: Relative amplitude and phase of the electric current produced by short-circuited element on a canonical structures for sub 6 GHz band

In the table 5.1, characterizing results for the canonical structure, a sphere and a cylinder is presented for 3 different values of the frequency of sub 6 GHz band. All of the figures presented are the representation of resulting amplitude and the phase of electric field produced by the corresponding passive radiation element. In first two rows the amplitude and the phase produced over a sphere for different value of frequency are presented respectively. Followed by this, results for cylinder is presented for a similar approach.

As can be seen above, as the value of the frequency increases, the resolution of the imaging improves providing the better information of the current distribution over the geometrical structure. It can be observed clearly in the representation of the amplitude, where the illuminated region (yellow color) is reduced when the value of the frequency is increased. In other hand, outcome of the phase representation is similar to the stationary wave produced over the geometrical structure by set of transmitters and receivers. As can be observed in the figures above, propagation of the phase corresponding to the distance can be seen. Over the both geometrical structure for each value of the frequency, the initial point of the propagation of the phase is the closer equivalent distance from the position of the transmitters and receivers.

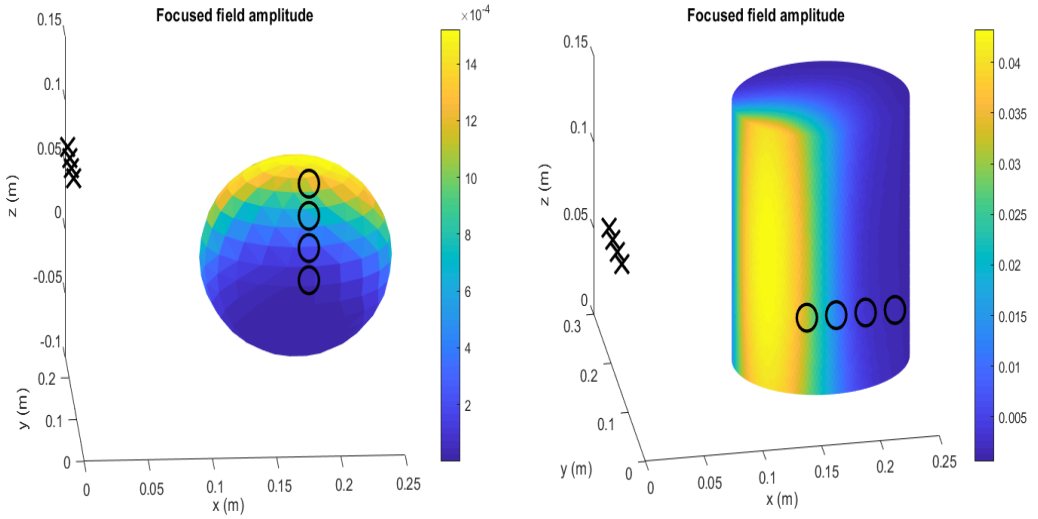

(A) Monopole on the top (B) Dipole on the lateral part

FIGURE 5.4: Signature of the radiating element over canonical vehicular platform for the frequency 4 GHz

Signature of the radiating element over a platform can be observed in the figure 5.4. In one case, on the surface of the sphere, the resulting illumination is the magnitude of the relative amplitude of the electric field produced by the radiating antenna 5.4a. In another case, obtained result is due to the presence of a radiating element on the lateral part of the platform 5.4b. These positions of the radiating antenna over two different platform corresponds to the illustration as in figure 5.1.

5.2.2 mmWave Band

For the identical geometric structures, similar study is done for the mmwave band. The main objective of this study, in particular, is to study the characterization for this band with better spatial resolution due to the higher value of the frequency.

Data	26 GHz	28 GHz	30 GHz
Amplitude	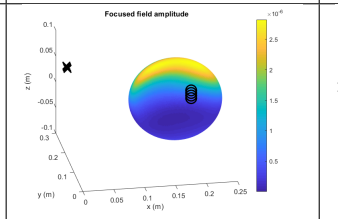	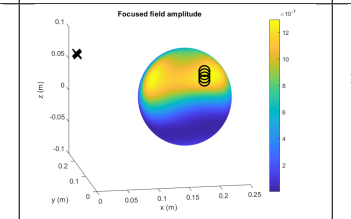	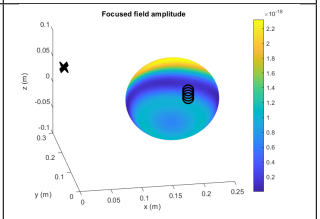
Phase	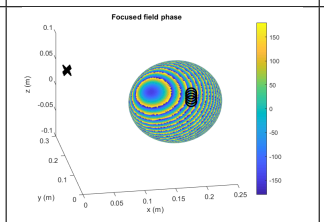	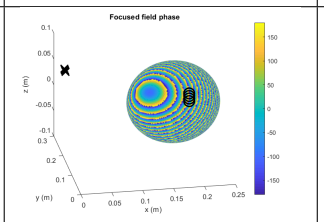	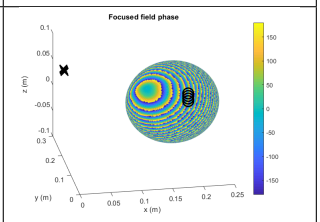
Amplitude	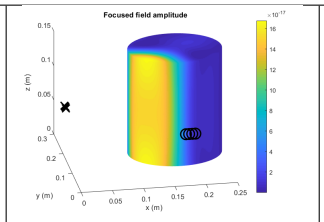	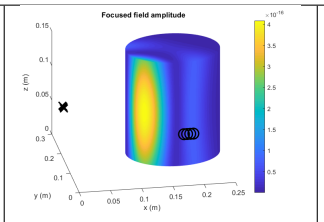	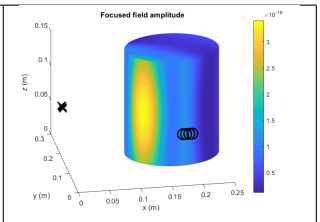
Phase	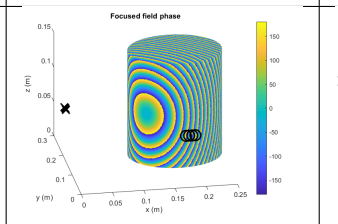	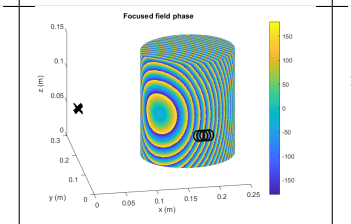	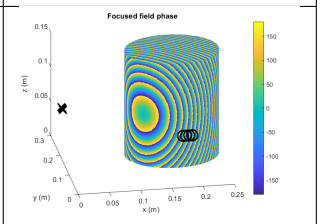

TABLE 5.2: Relative amplitude and phase of the electric current produced by short-circuited element on a canonical structures for mmwave band

For a mmwave band, the presented results as in table 5.2, illustrates the characterization of the electric effects produced by the passive element with better resolution. In the figures above, as can be seen the change of the phase is very fast due to the higher value of the frequency which improves the resolution as the wavelength is smaller. The improvement of the resolution of the amplitude as the frequency increases can be observed more clearly in case of the cylinder, where the illuminated region is smaller for the highest frequency.

5.3 Characterization of a Vehicle

Instead of the canonical structures, a characterization of a vehicle is done to study the the distribution of the electric current produced by the passive element. Below results for the sub 6 GHz band are presented.

Data	2 GHz	3 GHz	4 GHz
Amplitude	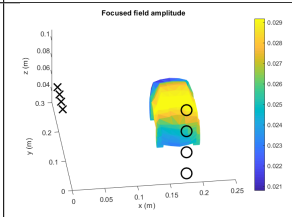	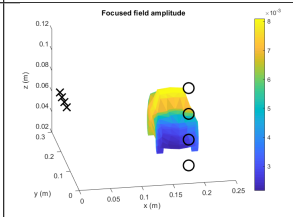	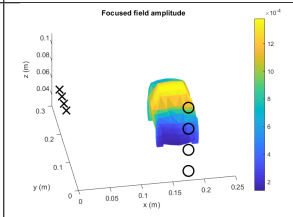
Phase	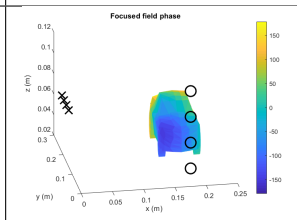	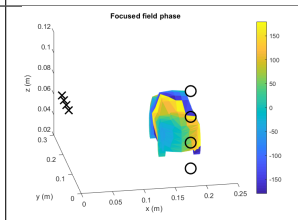	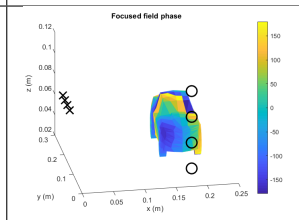
Amplitude	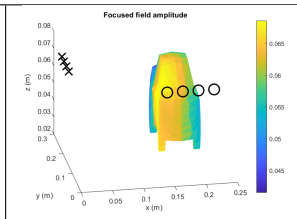	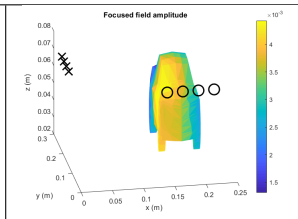	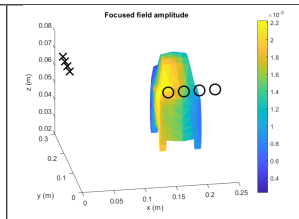
Phase	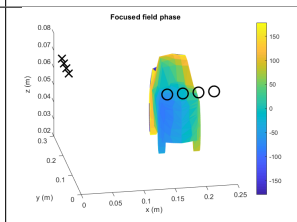	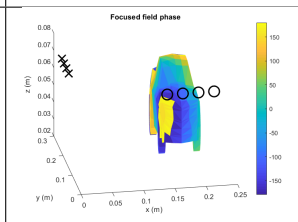	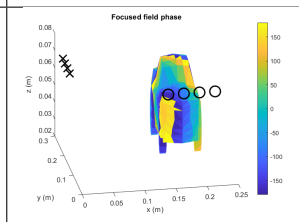

TABLE 5.3: Relative amplitude and phase of electric current produced by short-circuited element on a vehicle for sub 6 GHz band

First two rows provides the results for a vehicle with a passive element on a roof and last two rows represents the result for a vehicle with a passive radiating element on the lateral part of the car. Figures illustrating the amplitude, which represents the magnitude of the relative amplitude of the equivalent electric current generated due to the re-radiation of the passive elements. Similarly as before, the improvement of the resolution of the representation of the amplitude can be observed when increasing the frequency. Corresponding area, nearer to the passive radiating element, is illuminated with higher magnitude which can be considered as the distribution of the equivalent electric current.

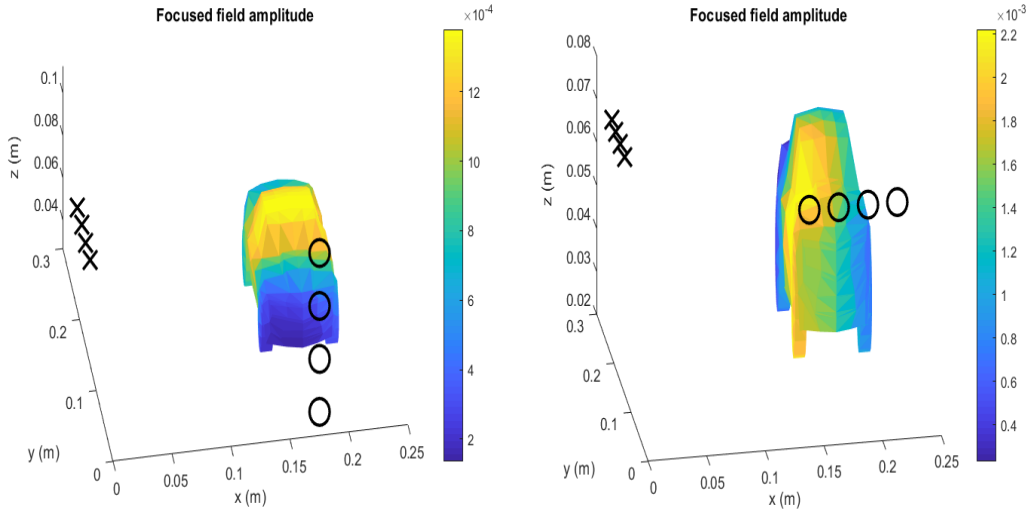

(A) Monopole on the roof of the car (B) Dipole on the side mirror

FIGURE 5.5: Signature characterization of a radiating element over a car for the frequency 4 GHz

As represented by the figure 5.5a, normalized amplitude of the distribution of the electric current produced by the radiating element placed at the top of the car can be seen. To extract the electromagnetic information, sensor antennas were placed orthogonally on a different plane, XY and XZ to have the resolution on the roof of the vehicle. This distribution can be considered as of the active radiating element. On the other hand, in figure 5.5b, the signature of a radiating element placed on the side mirror of the car can be seen. In this case, sensor antennas were placed orthogonally on a same plane i.e. XY to have the resolution of the lateral part of the vehicle

These positions of the antennas are most common these days being deployed in the car for a various communication purpose. Electromagnetic information of such scenario can be studied through this approach.

5.4 Experimental Validation

In this point, after having studied through the pre-experimental approach the signature of the radiating antenna over different vehicular platforms. Experimental analysis is done to validate the feasibility of the proposed concept.

5.4.1 Scenario Setup for Measurement

A simple scenario is setup to obtain the characteristics of the electromagnetic propagation of the scenario for two cases of measurement which are, electric field only with vehicle and electric field with a radiating element over the top of the vehicle. Measurements were done only to study the signature of the radiating antenna placed over the roof of the vehicle.

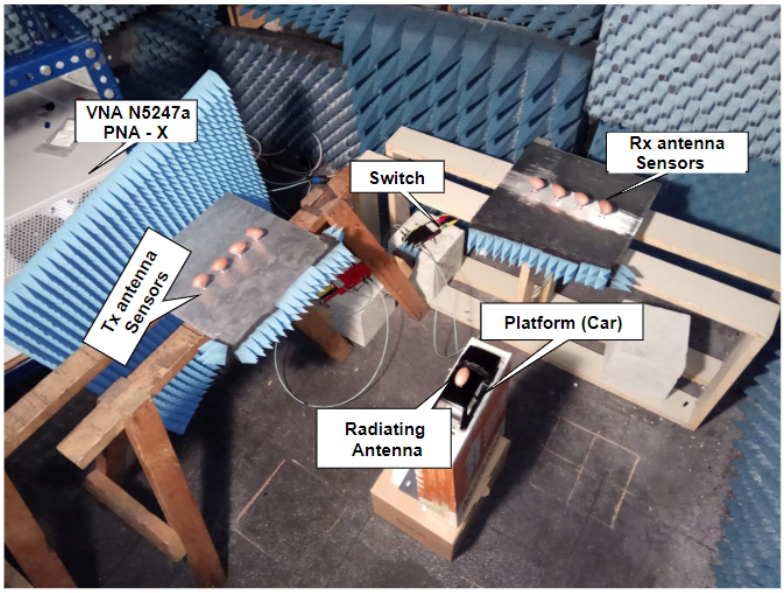

FIGURE 5.6: Characterization result for a car with antenna on a top for the frequency 4 GHz

Figure 5.6 shows the setup for the measurement inside the an-echoic chamber. The vehicle , a 1:25 scaled car, is placed on a support to be on a same height of the arrays of the sensor antennas. On the roof of the vehicle, a monopole antenna is placed short-circuiting with the roof of the vehicle which also acts as ground plane for the monopole antenna.

Used vehicle, a die cast car, is of dimension 25 cm $\times$ 6 cm $\times$ 5 cm with realistic parts like glassed windows and similar curves. After the post processing of the obtained data during the the measurement campaign, results representing the signature of the radiating antenna is plotted over the metallic rectangle of exact dimension as of the used car. This is done to plot the signature only on the surface.

Even though this specific type of scenario was modeled previously in pre-experimental approach with the sensor antennas on different orthogonal plane for the better resolution, in this experimental approach those antennas are place on same orthogonal plane for the simpler setup.

5.4.2 Results

Obtained results in MATLAB are presented below for the sub 6 GHz band. Resulting amplitude and the phase of the signature of the radiating antenna is presentet in table below.

Data	2 GHz	3 GHz	4 GHz
Amplitude	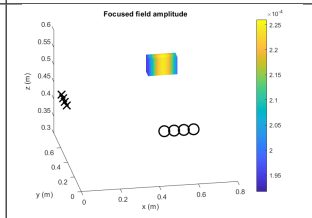	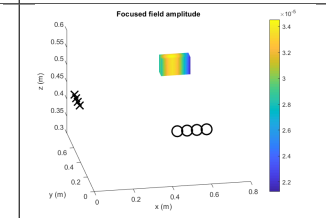	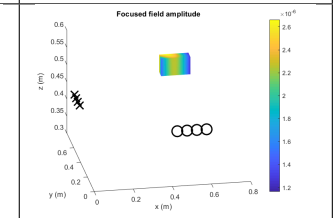
Phase	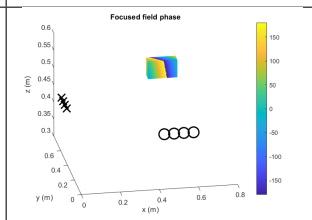	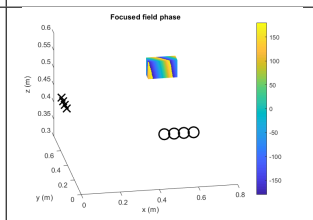	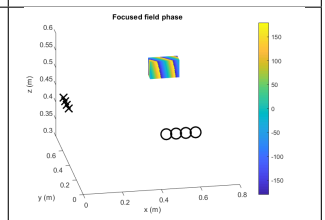

TABLE 5.4: Relative amplitude and phase of electric current produced by short-circuited element on a vehicle for 4 GHz

5.4.3 Amplitude of the Signature

Below, the magnitude of the amplitude of the signature of the radiating element is presented. The represented view is from the azimuth and the shown plane is the roof of the vehicle.

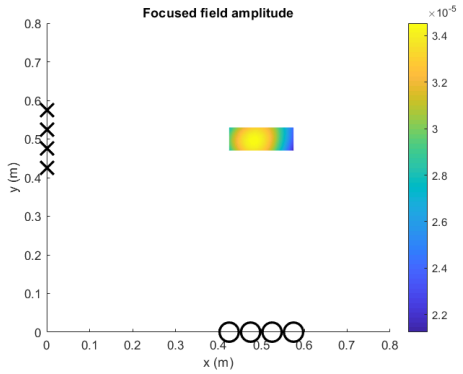

FIGURE 5.7: Relative amplitude representation over vehicle for sub 6 GHz band

In figure 5.7, resulting amplitude produced only in the presence of the radiating element on the roof is represented. This results shows the illuminated region, central part of the rectangle or equivalent to the roof, containing the signature of the radiating antenna.

Chapter 6

Conclusions

This chapter concludes the presented research work in this thesis. Furthermore, potential directions for future work are proposed.

In this thesis, a feasible method is proposed for the characterization of a vehicular platform scattering, but applicable to any generic geometrical structure.

Exploiting the RF imaging concept used by tomographic radars, distribution of the electric current produced over the geometrical structures was studied to validate the method. It is deduced that for this type of characterization, frequency band is very significant as the resolution of the characterization depends on the wavelength.

To validate the proposal of characterization, taking in account the projection of vehicular communication based on 5G, characterization of the vehicle with a radiating element for two potential frequency bands was studied. Results obtained after the post processing of data obtained from the theoretical, simulation and experimental approach were presented. Every aspects of these approaches were explained in detail.

It is shown that the used method for the characterization proposal can provide some significant outcome that can be used for the positioning of the antenna on the vehicle. The main advantage of using RF imaging technique is that, details of the characteristics of the electric field produced such as distribution of the equivalent current can be obtained without a sophisticated measurement systems with probes.

Further study is required for the improvement and to design an upgraded setup of the measurement systems for the higher frequency bands. The main improvement that can be done as a continuation of this work is to correct the anomaly appeared in the results. Different antennas can be used, for example multi frequency antennas instead of monopoles. Amortization of some process done during the measurement campaign can also bring a significant improvement on the results. Research on equipment and setup to be able to perform the characterization up to 60 GHz band will be interested follow up of this project. Also, one of the future work can be , study the the detection (RF imaging) and the characterization in a realistic scenario for example a indoor scenario with other electrically considerable objects on the surrounding.

Bibliography

[1] Nelson Patrick. Just one autonomous car will use 4,000 gb of data/day. *Network World*, 2016.

[2] Ángel Cardama, Lluis Jofre, Juan M Rius, Jordi Romeu, Sebastián Blanch, and Miguel Ferrando. Antenas. *Edicions de la Universitat Politècnica de Catalunya,*, 2002.

[3] Z. Yun and M.F. Iskander. "ray tracing for radio propagation modeling: Principles and applications. *IEEE Access*, 3:1089–1100, 2015.

[4] William C Jakes and Donald C Cox. *Microwave mobile communications*. Wiley-IEEE Press, 1994.

[5] Christian Ballesteros. 5g microwave vs. millimeter-wave mimo wireless mobile systems. Master's thesis, Universitat Politècnica de Catalunya, 2019.

[6] Kushal Dumre. Vehicle to vehicle (v2v) wireless communications, Bachelors Thesis, Universitat Politècnica de Catalunya, 2017.

[7] W. Sun, E. G. Ström, F. Brännström, Y. Sui, and K. C. Sou. D2d-based v2v communications with latency and reliability constraints. In *2014 IEEE Globecom Workshops (GC Wkshps)*, pages 1414–1419, Dec 2014.

[8] R. K. Mueller, M. Kaveh, and G. Wade. Reconstructive tomography and applications to ultrasonics. *Proceedings of the IEEE*, 67(4):567–587, April 1979.

[9] L. Jofre, A. Broquetas, J. Romeu, S. Blanch, A. P. Toda, X. Fabregas, and A. Cardama. UWB Tomographic Radar Imaging of Penetrable and Impenetrable Objects. *Proceedings of the IEEE*, 97(2):451–464, 2 2009.

[10] M. Pastorino. Short-range microwave inverse scattering techniques for image reconstruction and applications. *IEEE Transactions on Instrumentation and Measurement*, 47(6):1419–1427, Dec 1998.

[11] Yoo Jin Kim, L. Jofre, F. De Flaviis, and M. Q. Feng. Microwave reflection tomographic array for damage detection of civil structures. *IEEE Transactions on Antennas and Propagation*, 51(11):3022–3032, Nov 2003.

[12] Zhipeng Chen, Yuanjian Liu, Shuangde Li, and Guanyun Wang. Study on the multipath propagation characteristics of uwb signal for indoor lab environments. In *2016 IEEE International Conference on Ubiquitous Wireless Broadband (ICUWB)*, pages 1–4. IEEE, 2016.

[13] D. McNamara, C. Pistorius, and J. Malherbe. The uniform geometrical theory of diffraction. *Artech House, London*, 1990.

[14] Z. Yun and M. F. Iskander. Ray tracing for radio propagation modeling: Principles and applications. *IEEE Access*, 3:1089–1100, 2015.

[15] G. Spencer and M.Murty. General ray-tracing procedure. *JOSA*, 52(6):672–678, 1962.

[16] C. E. Shannon. A mathematical theory of communication. *Bell System Technical Journal*, 27(3):379–423, 1948.

[17] M Foschini, G. Gans. M. wireless personal communications. *Bell System Technical Journal*, 6(3):311–355, 1998.

[18] Shangbin Wu. Massive mimo channel modelling for 5g wireless communication systems, 2015.

[19] E. Telatar. Capacity of multi-antenna gaussian channels. *European Transactions on Telecommunications*, 10(6):585–595, 1999.

[20] D.S. Shiu, G. J. Foschini, M. J. Gans, and J. M. Kahn. Fading correlation and its effect on the capacity of multielement antenna systems. *European Transactions on Telecommunications*, 4:502–5513, 2000.

[21] Wikipedia . Eigenvalues and eigenvectors — Wikipedia, the free encyclopedia. https://en.wikipedia.org/w/index.php?title=Eigenvalues_and_eigenvectors&oldid=893666725, 2019.

[22] Lloyd N Trefethen and David Bau III. *Numerical linear algebra*, volume 50. Siam, 1997.

[23] A. Papió, A. Grau, J. Balcells, J. Romeu, L. Jofre, and F. De Flaviis. 60 GHz channel characterization using a Scatterer Mapping Technique. In *Proceedings of the Fourth European Conference on Antennas and Propagation*, pages 1–5, 4 2010.

[24] G.H. Golub, C.F. Van Loan, and P.C.F. Van Loan. *Matrix Computations*. Johns Hopkins Studies in the Mathematical Sciences. Johns Hopkins University Press, 1996.

[25] A. Papió, F. De Flaviis, L. Jofre, and J. Romeu. MM-wave scattering measurements for imaging and channel characterization. In *2012 6th European Conference on Antennas and Propagation (EUCAP)*, pages 3694–3698, 3 2012.

[26] Andreas Pfadler. Multi-antenna configuration modeling for massive mimo v2i. Master's thesis, Universitat Politècnica de Catalunya, 2019.

[27] Christian Ballesteros, Kushal Dumre, Badr Bouazza, and Lluis Jofre. Sub-6 ghz vs ka band multi-antennaindoor scattering characterization. In *XXXIV Simposio Nacional de la Unión Científica Internacional de Radio*, pages 1–4. URSI, 2019.

Appendix A

Contributions

As the outcome of this project, in collabration with the supervisor and the mentor of this thesis, following paper was presented in Simposium de la Union Cientifica Internacional de Radio, 2019 (URSI), which is accepted to be published (Contribution id 248).

Sub-6 GHz vs Ka Band Multi-Antenna Indoor Scattering Characterization

C. Ballesteros[(1)], K. Dumre[(1)], B. Bouazza[(1)], M.T. Martinez-Inglés[(2)],
J.V. Rodríguez[(2)], J.M. Molina[(2)], J. Romeu[(1)], L. Jofre[(1)]
christian.ballesteros@tsc.upc.edu, josemaria.molina@upct.es, romeu@tsc.upc.edu, jofre@tsc.upc.edu
[(1)]Signal Theory and Communications Department. Universitat Politècnica de Catalunya. UPC Campus Nord, Barcelona, Spain
[(2)]Depto. Tecnologías de la Información y las Comunicaciones. Universidad Politécnica de Cartagena. Cartagena, Murcia, Spain

***Abstract*—In this paper, sub-6 GHz and millimeter-wave (mmW) band channel scattering characterization are performed and imaging reconstruction is obtained by using a 2-D scatterer mapping technique based on Multi-frequency Bi-focusing (MF-BF). The data matrix is also processed to obtain its eigenvalues and eigenvectors. A relation between the eigenvalues and the number of scatterers and the eigenvectors and the scatterers spatial localization is obtained.**

I. Introduction

With the progressive deployment of the 5G and its growing needs for higher capacities, the frequency spectrum is exploited at sub-6GHz and extended to millimeter-wave ranges. Both bands have their specific characteristics in terms of capacity (higher at higher frequencies), coverage (better at lower frequencies) and positioning (robustness of the location, potentially better at lower frequencies, and accuracy, potentially better at higher frequencies).

In this paper, the scattering properties of an indoor scenario are characterized at both sub-6GHz (3–4 GHz) and mmW frequencies (24-30 GHz). Different channel parameters are extracted, as well as the process to obtain the reconstructed image. A 2D scatterer sensing and mapping technique based on a MF-BF is applied to reconstruct the presented scenarios. The scattered field matrices are post-processed also to obtain their eigenvalues and eigenvectors and relate them to the spatial distribution of the scatterers on the area under reconstruction.

II. 2D Scatterer Mapping Technique

The general idea for the Scatterer Mapping technique [1], [2] consists in distributing a certain number of microwave sensors (transmitters and/or receivers) on a certain region, covering as much as possible the area under investigation, as shown in figure 1. The goal is to obtain the spatial and electrical information of the extended object ε_r relative to the original background constant ε_b of the interrogation area S_o. The object can be a continuous distribution or a discrete set of objects S_k with electrical permittivity $\varepsilon_{S_k}(\vec{r})$.

The equivalent electric current distribution that is induced when the scatterer is illuminated with an electromagnetic field generated by the transmitter located at $\vec{r}_{T_i}$ at a frequency f, i.e., $E(\vec{r}, f; \vec{r}_{T_i})$, is proportional to the electrical contrast $c(\vec{r}) = (\epsilon_t(\vec{r}) - \epsilon_b)/\epsilon_b$ and it is defined as:

$$J_{eq}(\vec{r}, f; \vec{r}_{T_i}) = j\omega\epsilon_b c(\vec{r}) E(\vec{r}, f; \vec{r}_{T_i}) \tag{1}$$

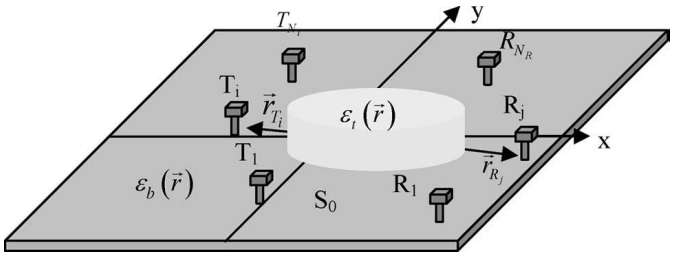

Fig. 1: Scatterer Mapping Technique Sensing Geometry

A set of M_T transmitters and M_R receivers are used to scan the interrogation area where the reconstruction algorithm is applied. First, the information (or channel) matrix E is obtained as follows. For every transmitting element, the receiving array is scanned over each receiving element, obtaining an M_R measurement vector. This procedure is done for all M_T transmitting elements, thus to obtain $M_T \times N_R$ matrix. The scattered field captured by a receiver positioned at $\vec{r}_{R_j}$ created by the equivalent current $J_{eq}(\vec{r}, f; \vec{r}_{T_i})$ can be expressed as:

$$E_s(\vec{r}_{R_j}, f, \vec{r}_{T_i}) = -j\omega\mu_0 \int_{Vo} J_{eq}(\vec{r}, f; \vec{r}_{T_i}) G(|\vec{r}_{R_j} - \vec{r}|, f) dV\,, \tag{2}$$

where $G(|\vec{r}_{R_j} - \vec{r}|, f)$ is the Green's function. Vertical formulation based on 3-D Green function should be used to compensate the effects like vertical diffraction and depolarisation, caused due to the object inhomogeneities in the z-axis. Additionally, the scattered field E_s may be expressed as in equation 3, where E_{total} is the electric field with the presence of scatterer and $E_{background}$ is the electric field without any object in the scenario.

$$E_s = E_{total} - E_{background} \tag{3}$$

For the reconstruction of the scatterer, image points of the scenario are formed by means of synthesising two groups of focused antennas (transmitting and receiving). The resulting scattered field matrix E_s is mathematically treated with corresponding weights, using the focusing algorithm over each specific point of the reconstruction area. This focusing algorithm restores the changes in phase and amplitude of waves travelling from transmitting antenna to the analyzed point and then to the receiving antenna. These electromagnetic waves suffer refraction and diffraction due to the presence

of the scatterer. Applying this focusing algorithm on the channel matrix for all points of the space grid, a replica of the environment to be reconstructed is obtained.

The system provides also useful information for the characterization of the wireless channel by obtaining parameters such as the eigenvalues and eigenvectors of the scattered fields matrix [3]. Following the same approach as in [4], the Singular Value Decomposition (SVD) is applied to the scenario under investigation.

$$E_{SM_T \times M_R} = U_{M_T \times M_T} S_{M_T \times M_R} V^T_{M_R \times M_R} \tag{4}$$

where the columns of U are the left eigenvectors related to the transmission array, S is a diagonal matrix including the eigenvalues and V^T is the transpose matrix of the right eigenvectors, related to the receiving array.

III. Indoor Scenario

The scenario considered in this study is depicted in Fig. 2. Three dielectric cylinders of 50 mm of diameter are spread over a 0.5 m×0.5 m room. Two orthogonal arrays of 5 elements each are placed at two edges of the scenario, centered with respect each dimension, with an inter-element separation of $d_{Tx} = d_{Rx}$. For the low frequency band (3–4 GHz), the distance is 50 mm, whereas for the higher band (24–30 GHz) is 5 mm, corresponding to the half-wavelength values at the respective lowest and highest frequency.

The particular dielectric properties of the cylinders are discussed in section IV.

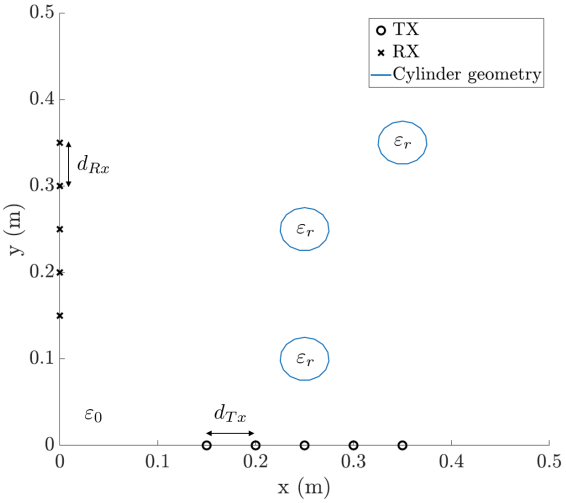

Fig. 2: Indoor Scenario for simulation

IV. Numerical Results

The algorithm is performed over different scenarios in order to validate its performance under several conditions. The focusing capabilities are tested and some parameters such as the Multiple-Input and Multiple-Output (MIMO) channel eigenvalues and eigenvectors are analyzed to obtain relevant information about the scatterers. The number of frequency samples is kept constant for both frequency bands ($N_f = 11$), corresponding to steps of $\Delta f_{low} = 100\,MHz$ and $\Delta f_{high} = 600\,MHz$ for the lower and upper bands.

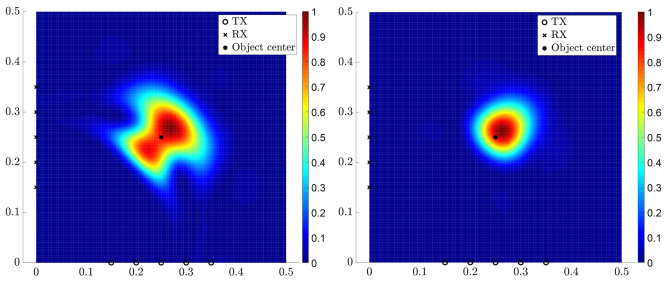

(a) $\varepsilon_r = 2.5$ (b) $\varepsilon_r = 10$

Fig. 3: Single cylinder focusing for 3–4 GHz band for two different permittivity values.

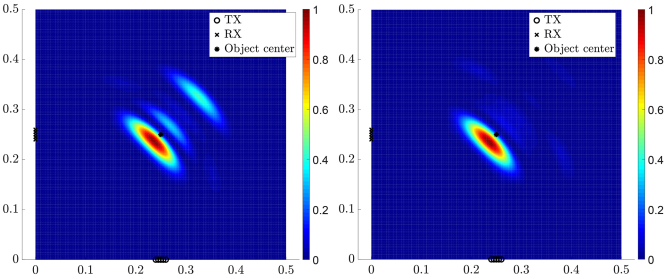

(a) $\varepsilon_r = 2.5$ (b) $\varepsilon_r = 10$

Fig. 4: Single cylinder focusing for 24–30 GHz band for two different permittivity values.

The first case under study concerns the use of the two frequency bands under investigation, i.e., 3–4 GHz and 24–30 GHz to model the geometry of a single scatterer. In addition, two situations are considered: low and high dielectric constant ($\varepsilon_{r,low} = 2.5$ and $\varepsilon_{r,high} = 10$). The focusing for the lower frequency band is depicted in Fig. 3. The dielectric cylinder is properly reconstructed when high permittivity is assumed, whereas the pattern is distorted for the low permittivity cylinder. In Fig. 4, the same analysis is performed for the upper frequency band. The influence of the dielectric properties of the cylinder is not as high as in previous case. Now, the circular section is not shown, but a flattened projection in the diagonal axis covering only a small section of the cylinder.

Once the focusing capabilities of the system are analyzed, the complete scenario is deployed including the three dielectric cylinders. From this point forward, only the case of high permittivity material is considered. Fig. 5 shows the focused fields for the two frequency bands, for which the same analysis of the single scatterer case can be extended.

The scattered fields matrix is normalized by means of the Frobenius norm and then decomposed into the singular vector and value matrices. Fig. 6 depicts the evolution of the eigenvalues over the lower frequency range for the case of one and three cylinders in the scenario, whereas Fig. 7 presents the equivalent values for the upper band. It can be observed that each scatterer contributes with an eigenvalue whose level depends on the relative illumination among them.

Finally, the eigenvectors associated to the main eigenvalues, one for each scatterer present in the scenario, are used to spatially locate the dielectric cylinders. They are taken as the amplitude and phase of the array weights. In particular, the left

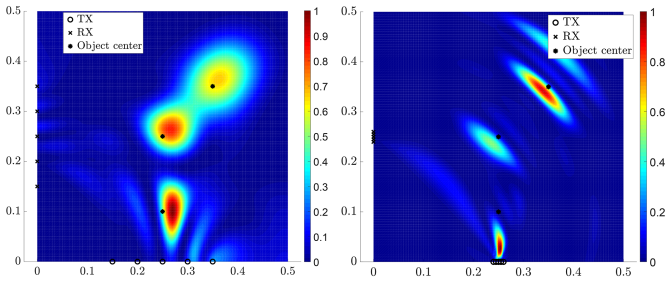

(a) 3–4 GHz (b) 24–30 GHz

Fig. 5: Focused fields of the three-scatterer scenario at the two frequency bands.

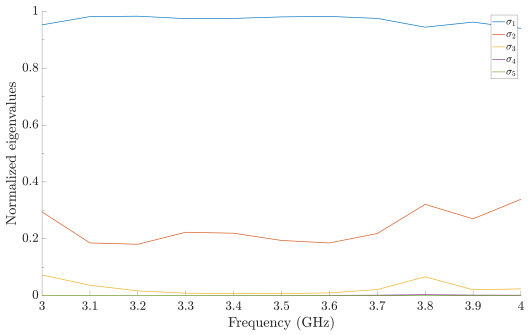

(a) One cylinder

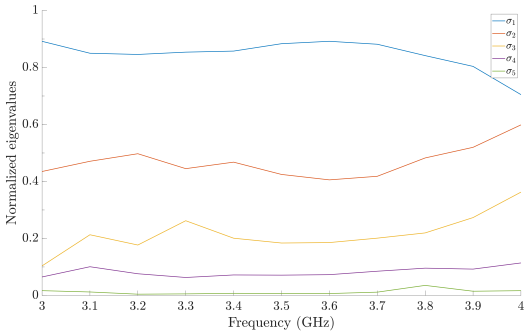

(b) Three cylinders

Fig. 6: Distribution of the scattered field matrix eigenvalues between 3 and 4 GHz when (a) one or (b) three cylinders with $\varepsilon_r = 10$ are present.

eigenvectors generate the radiation pattern of the transmitter array and the right eigenvectors, the receiving one. Fig. 8 and Fig. 9 show those patterns at the central frequency of the two studied bands, i.e., 3.5 GHz and 27 GH, respectively.

The patterns are degraded by the presence of the other scatterers and in some cases there is not a clear maximum towards the real direction of the cylinder. The diagrams corresponding to the lower eigenvalues are the most affected and it is difficult to discern the exact position of the scatterer.

V. Conclusion

In this paper, the capabilities of the MF-BF imaging algorithm and the SVD technique are discused to obtain the spatial reconstruction of dielectric scatterers present in a certain area of interest.

The proposed system is based on two orthogonal arrays which focus the region where the scatterers are located to

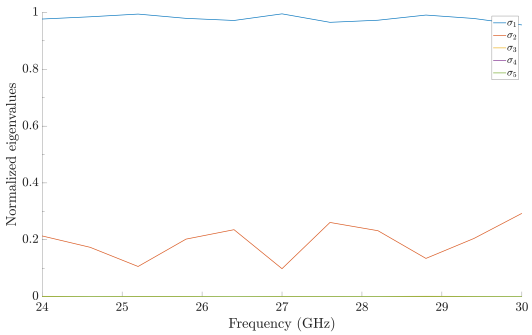

(a) One cylinder

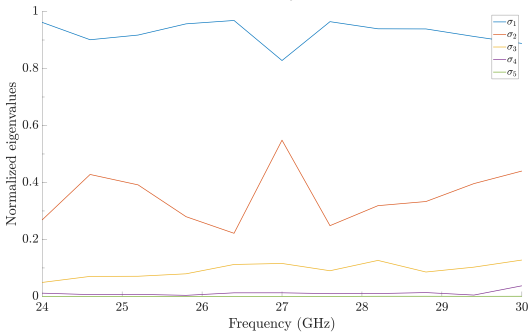

(b) Three cylinders

Fig. 7: Distribution of the scattered field matrix eigenvalues between 24 and 30 GHz when (a) one or (b) three cylinders with $\varepsilon_r = 10$ are present.

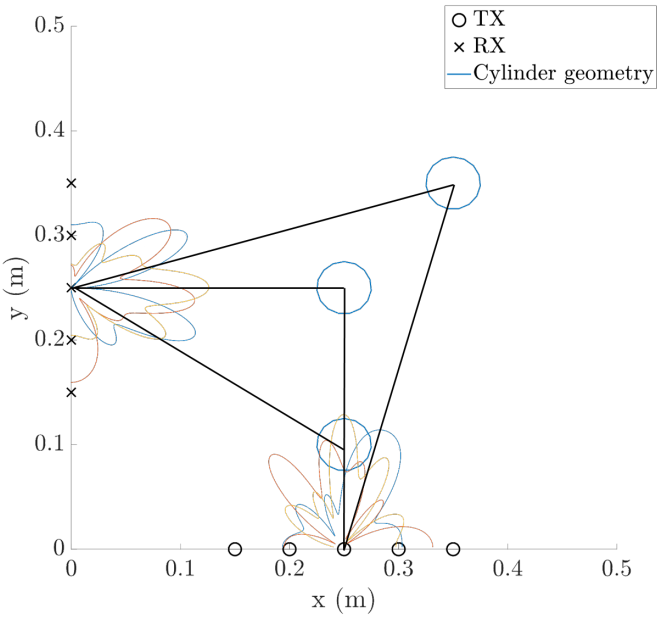

Fig. 8: Radiation patterns of the equivalent arrays weighted with the eigenvectors of the scattered fields matrix ($f = 3.5\,GHz$)

create a recontructed image of the environment. The study is extended to two frequency bands, one in the sub-6 GHz region and another close to the mmW band. The impact of the scatterer dielectric properties in the resulting image is also analyzed.

The number of channel matrix eigenvalues clearly different from zero is an indicator of the reflectivity of the environ-

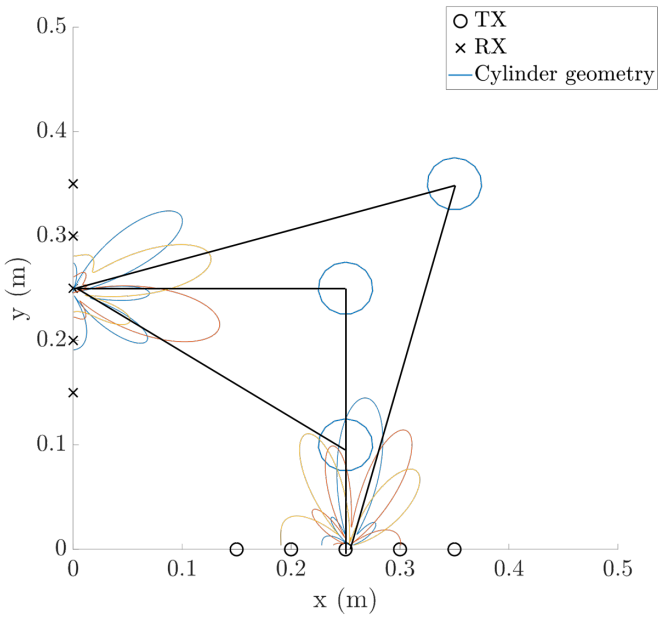

Fig. 9: Radiation patterns of the equivalent arrays weighted with the eigenvectors of the scattered fields matrix ($f = 27\,GHz$)

ment and the number of main scattering points. Moreover, the eigenvalues level provide an intuitive perception of the strength of the scattered fields by each scatterer. The matrix eigenvectors are used to weight each antenna element on the transmitting and receiving arrays to locate each scatter.

The potential of the singular value decomposition in understanding the channel propagation characteristics has also been highlighted.

ACKNOWLEDGEMENT

This work was partly funded by Colciencias through Convocatoria 727 of 2015, the Ministerio de Economía y Competitividad under projects TEC2016-78028-C3-1-P, TEC2016-78028-C3-3-P, MDM2016-O6OO, Catalan research Group 2017 SGR 219. The Spanish Ministry of Education contributes via a doctoral grant to the first author (FPU17/05561)

REFERENCES

[1] L. Jofre, A. Broquetas, J. Romeu, S. Blanch, A. P. Toda, X. Fabregas, and A. Cardama, "UWB Tomographic Radar Imaging of Penetrable and Impenetrable Objects," *Proceedings of the IEEE*, vol. 97, no. 2, pp. 451–464, 2 2009.

[2] A. Papió, A. Grau, J. Balcells, J. Romeu, L. Jofre, and F. De Flaviis, "60 GHz channel characterization using a Scatterer Mapping Technique," in *Proceedings of the Fourth European Conference on Antennas and Propagation*, 4 2010, pp. 1–5.

[3] G. H. Golub and C. F. Van Loan, *Matrix computations*. JHU press, 2012, vol. 3.

[4] A. Papió, F. De Flaviis, L. Jofre, and J. Romeu, "MM-wave scattering measurements for imaging and channel characterization," in *2012 6th European Conference on Antennas and Propagation (EUCAP)*, 3 2012, pp. 3694–3698.